Astronomy & Astrophysics manuscript no. astroph
February 15, 2012

MASSIV: Mass Assembly Survey with SINFONI in VVDS ⋆

IV. Fundamental relations of star-forming galaxies at $1 < z < 1.6$⋆⋆

D. Vergani[1,2], B. Epinat[3,4,5], T. Contini[3,4], L. Tasca[5], L. Tresse[5], P. Amram[5], B. Garilli[6], M. Kissler-Patig[7], O. Le Fèvre[5], Moultaka, J.[3,4], Paioro, L.[6], J. Queyrel[3,4], and C. López-Sanjuan[5]

[1] INAF-IASFBO, Via P. Gobetti 101, I-40129 Bologna, Italy, e-mail: vergani@iasfbo.inaf.it
[2] INAF-Osservatorio Astronomico di Bologna, Via C. Ranzani 1, I-40127 Bologna, Italy
[3] Institut de Recherche en Astrophysique et Planétologie (IRAP), CNRS, 14 Avenue Édouard Belin, F-31400 Toulouse, France
[4] IRAP, Université de Toulouse, UPS-OMP, F-31400 Toulouse, France
[5] Laboratoire d'Astrophysique de Marseille, Université d'Aix-Marseille, CNRS, 38 rue Frédéric Joliot-Curie, F-13388 Marseille Cedex 13, France
[6] INAF-IASFMI, Via E. Bassini 15, I-20133 Milano, Italy
[7] ESO, Karl-Schwarzschild-Str. 2, D-85748 Garching b. München, Germany

Received —; accepted —

ABSTRACT

Aims. How mass assembly occurs in galaxies and which process(es) contribute to such activity are some of the main questions highly debated in galaxy formation and evolution theories. This has motivated our survey MASSIV (Mass Assembly Survey with SINFONI in VVDS) of $0.9 < z < 1.9$ star-forming galaxies selected from the purely flux-limited VVDS redshift survey.

Methods. We evaluate the characteristic size and stellar mass of 45 MASSIV galaxies at $1 < z < 1.6$ and we use the internal dynamics obtained with the SINFONI/VLT-ESO integral field spectrograph, in order to derive the stellar mass - size - velocity relations. We use the Kennicutt-Schmidt formulation to estimate the gas content and to compute its contribution to the total baryonic mass in MASSIV galaxies.

Results. For the first time we obtain the relations between galaxy size, mass, and internal velocity, and the baryonic Tully-Fisher relation, from a statistically representative sample of star-forming galaxies at $1 < z < 1.6$. We derive a dynamical mass which is in good agreement with rotating galaxies containing a gas fraction of $\sim 20\%$, that is perfectly consistent with the content derived using the Kennicutt-Schmidt formulation and corresponding to the expected evolution. Non-rotating galaxies are more compact in their extent of the stellar component, and less massive than rotators, but not statistically different in their gas extent. We obtain a marginal evolution in the size - stellar mass and size - velocity relations with discs being evenly smaller with cosmic time at fixed stellar mass or velocity, and less massive for a given velocity with respect to the local Universe. This result does not imply an abnormal evolution in the galactic spin as previously reported. The scatter of the Tully-Fisher relation is reduced introducing the S_{05} index, that is interpreted with the increasing contribution to galactic kinematics of turbulent motions with cosmic time. We report a persisting scatter for rotators in our relations, that we suggest to be intrinsic, and possibly caused by complex physical mechanism(s) at work in our stellar mass/luminosity regime and redshift range.

Conclusions. Our results consistently point towards a mild, net evolution of these relations, comparable to what is predicted by cosmological simulations of disc formation. In a conflictual picture where earlier studies reported discrepant results, our findings put on firmer ground the lack of an influential transformation of the fundamental relations of star-forming galaxies for at least 8 Gyr and a dark halo strongly coupled with galactic spectrophotometric properties.

Key words. Galaxies: high-redshift - galaxies: evolution - galaxies: kinematics and dynamics - galaxies: fundamental parameters

1. Introduction

In the current paradigm of structure formation, galaxies are formed in dark matter halos which grow along cosmic time via hierarchical assembly of smaller units. While halo−halo merging is the main physical process driving the assembly of dark−matter halos and successfully describes the galaxy clustering properties, it is unclear how it affects the build−up of galaxies, and how other physical processes might play a role.

With considerable efforts, large and deep spectroscopic surveys of local and higher−z galaxies have been performed in the last decade to understand galaxy formation and evolution. Among the many trends that have been found between various galaxy properties (e.g., luminosity, colour, stellar mass, surface brightness, star−formation rate) a general consensus has been reached on a luminosity/mass−dependent evolution of the distribution functions (e.g. Zucca et al. 2006; Pozzetti et al. 2007; Bundy et al. 2006; Fontana et al. 2004, 2006) supporting the downsizing scenario (e.g. Cowie et al. 1996).

Send offprint requests to: D. Vergani, e-mail: *vergani@iasfbo.inaf.it*

⋆ This work is based mainly on observations collected at the European Southern Observatory (ESO) Very Large Telescope, Paranal, Chile, as part of the Programs 179.A-0823, 177.A-0837, 78.A-0177, 75.A-0318, and 70.A-9007. This work also benefits from data products produced at TERAPIX and the Canadian Astronomy Data Centre as part of the Canada-France-Hawaii Telescope Legacy Survey, a collaborative project of NRC and CNRS.

⋆⋆ All the data published in this paper are publicly available following this link: http://cosmosdb.lambrate.inaf.it/VVDS-SINFONI

There is convincing evidence that $1 < z < 2.5$ is a critical cosmic time, when galaxy properties are evolving rapidly. During this period we witness an intense mass assembly activity along with a morphological differentiation of galaxies well underway. This epoch corresponds to the maximal star formation activity in the Universe around $z \sim 2$ (e.g. Tresse et al. 2007; Cucciati et al. 2011), and the fast build−up of the stellar mass observed in early−type galaxies at $z \sim 1 - 1.5$ (Arnouts et al. 2007; Vergani et al. 2008). It is also an epoch when the connection between AGN and star formation could play an important role in shaping galaxies. In this framework the knowledge of the dynamical state of galaxies is an indispensable information to assess the mechanisms governing the growth of luminous structures in the Universe.

In the last years the availability of integral field spectrographs working under excellent seeing conditions, or assisted by adaptive optics, has opened a new era in the investigation of galactic resolved dynamics at high redshifts, with integral field spectrographs bringing considerably more information than traditional long-slit techniques. Mapping the full two-dimensional velocity fields and velocity dispersion is essential in many dynamical studies in contrast with the classical long-slit technique: it avoids misinterpretation of the measured velocities due to the misalignment between the photometric and kinematic axis, or to large dispersion velocities. This is especially true at increasing look-back times when galaxies show a larger incidence of irregular shapes and chaotic motions. In addition, new opportunities have recently been opened in the near-infrared regime in which new instruments allow one to sample the rest-frame optical emission that contains all major diagnostic lines, e.g., SINFONI on VLT, Eisenhauer et al. (2003) and OSIRIS on Keck, Larkin et al. (2006). Spatially-resolved observations of UV/optically selected galaxies at $1.5 < z < 3$ (Genzel et al. 2006, 2008; Förster Schreiber et al. 2006, 2009; Bouché et al. 2007; Law et al. 2007, 2009; Wright et al. 2008; Stark et al. 2008; Epinat et al. 2009) together with cosmological simulations (e.g., Genel et al. 2008; Dekel et al. 2009) indicate that many of the physical properties of these sources cannot be primarily attributed to major merger events experienced in the history of galaxies. Instead internal mechanisms are contributing to mass assembly (Genzel et al. 2008, and references therein). In driving the observed dynamics, they can correspond to the infall of accreting matter, and/or large collisional clumps (e.g., Law et al. 2007, 2009; Genzel et al. 2011) and/or processes related with star formation (Lehnert et al. 2009).

In summary the emerging scenario is minimizing the importance of major merging in shaping up galaxies at early epochs, apparently at odds with the hierarchical assembly of mass in the cold dark matter paradigm - although merging systems are identified in about one third of the galaxies studied. A general consensus has not been reached yet (e.g., Robertson & Bullock 2008).

So far a detailed view of dynamics of distant galaxies is restricted to a limited number of objects caused primarily by the large investment of telescope time to build up a fair sample. The most efficient approach to this issue is to adopt certain selection techniques, such as various combinations of colours to focus on a specific redshift range and/or targeting extended discs to ensure sufficient spatial sampling (Law et al. 2007, 2009; Förster Schreiber et al. 2006, 2009). While pre-selecting galaxies remains the most effective way to gather a large, high-z galaxy catalogue, when exploring statistical issues it is highly desirable to have a fully representative catalogue of galaxies with well known selection functions on multiple fields of a homogeneous survey (e.g., Puech et al. 2010). Having a sufficient spatial resolution is also an issue as demonstrated by a survey such as IMAGES (Intermediate MAss Galaxy Evolution Sequence) that selects $z \sim 0.6$ galaxies observed with limited spatial resolution ($0\farcs52$ pix^{-1}). The resulting picture emerging from various data-sets offers discrepant results on the evolution of the fundamental relations between galaxy size, mass, and velocity (e.g., Flores et al. 2006; Puech et al. 2008, 2010; Bouché et al. 2007; Förster Schreiber et al. 2009; Cresci et al. 2009; Law et al. 2007, 2009). As these quantities represent important indicators to understand the structure and evolution of disc galaxies, the interpretation of their changes, or constancy in time, would imply a modification in the standard picture of galaxy disc formation. For instance, at odds with earlier findings and theoretical expectations, the absence of evolution in the size-velocity relation of disc galaxies reported by Bouché et al. (2007) have fundamental implications in the growth of the specific angular momentum of dark matter halos.

To overcome the above-mentioned difficulties and shed light on relations linking various galactic properties to dynamics, we are carrying on the MASSIV programme (Mass Assembly Survey with SINFONI in VVDS) to obtain near-infrared integral field spectroscopy of a hundred of star-forming galaxies selected with a pure flux limiting criterion on three VVDS fields. The main goal of MASSIV is to obtain a detailed description of galaxy dynamics to probe their formation and evolution in a representative sample of galaxies in the crucial $1 < z < 2$ epoch. In the first set of papers we present the survey in Contini et al. (2011), the kinematic classification of galaxies in Epinat et al. (2012), and their resolved metallicity in Queyrel et al. (2011). In the present paper, we present the fundamental scaling relations that exist among the mass, size, and velocity in galaxies.

In Sect. 2 we summarize our sample selection, observations and data reduction. In Sect. 3 we detail the procedures to determine the physical properties of the MASSIV galaxies (morphology, mass, star formation rate, kinematics inferred from the photometric and integral field spectroscopic data). In Sect. 4 we discuss the gas content and the size of our galaxies and in Sect. 5 we summarize the impact of our resulting scaling relations in the context of mass assembly.

Throughout this work we assume a standard cosmological model with $\Omega_M = 0.3$, $\Omega_\Lambda = 0.7$ and $H_0 = 70\,\mathrm{km\,s^{-1}\,Mpc^{-1}}$ (which gives a median scale of 8.32 kpc arcsec^{-1} at $z \sim 1.24$). Magnitudes are given in the AB system.

2. Observations

2.1. Sample selection

We report SINFONI (Eisenhauer et al. 2003; Bonnet et al. 2004) observations of our new resolved kinematic MASSIV survey. The galaxies have been selected from the VVDS. The VVDS is a redshift survey which has mapped and presented results on the evolution of galaxies, large scale structures, and AGNs from the spectroscopic identification of about 50,000 sources down to a limiting magnitude of $I_{AB} = 22$ in the Wide Fields (Garilli et al. 2008), to $I_{AB} = 24$ in the Deep Field (Le Fèvre et al. 2005), and to $I_{AB} = 24.75$ in the Ultra-Deep Field (see Tab. 1). The VVDS is combined with a multi-wavelength dataset from radio to X-rays.

The MASSIV sample analysed in this work was selected on the basis of several criteria (see details in Contini et al. 2011). They can be summarized as follows:

1) Galaxies with a redshift assigned to their rest-frame UV VVDS spectra at a confidence level larger than 80% in the red-

shift range $z = 0.9 - 1.8$ were pre-selected. The confidence level of the redshift determination has been estimated in the VVDS on the basis of repeated observations. Galaxies are grouped into four classes and we used only those that correspond to the maximum success probability of having an accurate redshift.

2) Their spectral features (H$\alpha\lambda$6563Å, or [OIII]λ5007Å) had to fall in a region not contaminated by OH sky-lines. Strong sky-lines were outdistanced by a minimum of 9Å from the above-mentioned spectral lines computed using our VIMOS spectroscopic redshifts. Thus, we could observe an OH-uncontaminated emission line with a typical rotation of 200 km s^{-1}.

3) Star-forming galaxies below $z < 1.46$ have been selected in taking a certain threshold in the equivalent width (EW) of the [OII]λ3727 doublet in VIMOS spectra with a signal-to-noise ratio (SNR) above 6. That is, $z < 1.46$ galaxies with EW[OII] larger than 25Å in SNR≤10 spectra and 40Å in $6 \leq SNR \leq 10$ spectra have been selected. Star-forming galaxies at higher redshifts have been selected using the rest-frame UV spectra. These constraints guarantee the detection of H$\alpha\lambda$6563Å (or [OIII]λ5007Å) in SINFONI spectra within the scheduled observing time.

Out of the $\sim 30,000$ spectra observed in the various VVDS fields, 10% of them satisfy these criteria (see Tab. 1 for the details). From this subsample 84 galaxies have been observed in the framework of MASSIV. The galaxy VVDS220148046 supposed to be at redshift 1.3710 based on the VIMOS spectrum turns out to have a redshift of 2.2442 identified with the Hβ and [OIII] lines in SINFONI observations. This galaxy is not included in the current analysis. Finally, our 83 galaxies are representative of the star-forming galaxy population at $0.9 < z < 1.8$ uniformly distributed in the stellar mass interval $\log\mathcal{M}/\mathcal{M}_{\odot} = 9.47 - 11.77$. In this sample ten galaxies have been observed with the adaptive optics (AO) system of SINFONI assisted with the Laser Guide Star (LGS) facility to achieve a better angular resolution.

In this analysis we are using more than half of the entire MASSIV sample, i.e., 49/83 galaxies, or about $\sim$ 60%. Thanks to the high precision of the VVDS redshifts, almost all observed galaxies have been detected (45/50) with either H$\alpha\lambda$6563Å (44/45) or [OIII]λ5007Å (1/45). In particular, with seeing-limited mode all but one (43 out of 44) galaxies targeted in H$\alpha\lambda$6563Å have been detected. Seven out of 50 galaxies have been observed with adaptive optics (out of which two have no detection, one targeted in Hα and the other one in [OIII]). The fifty galaxies that constitute the original MASSIV sample (see Tab. 1) have a median redshift of $z = 1.2423$ (where $z_{25\%} = 1.0375$ and $z_{75\%} = 1.3547$ are the two extreme quartiles of the redshift distribution). Excluding our serendipitous detection at $z = 2.2442$ and the four undetected galaxies, the median redshift of our 45 galaxies analysed in this work remains similar to the original sample ($z = 1.2246$ with $z_{25\%} = 1.0351$ and $z_{75\%} = 1.3338$).

Table 1. Sample selection.

VVDS Survey fields (1)	$I_{AB,lim}$ (2)	Number of targets (3)	Criteria Full-filled (4)	MASSIV sample (5)	This work (6)
Wide	17.5-22.50	24,507	224 (183)	21 (4)	21 (4)
Deep	17.5-24.00	12,668	2,600 (300)	29 (1)	27 (1)
Ultra-Deep	23.0-24.75	1,200	86 (55)	34 (6)	2 (2)

(1) The fields of the VVDS used in MASSIV. (2) I_{AB} limiting magnitude selection. (3) Total number of spectroscopic targets. (4) Number of targets fulfilling criteria described in Sect. 2.1. (5) Total number of galaxies in the MASSIV sample at the completion of the survey. (6) Number of galaxies used in this analysis.
In columns from (4) to (6) we indicate with parentheses the numbers of targets observed with adaptive optics in our observing campaign.

2.2. SINFONI Data Acquisition and Reduction

The observations of the MASSIV sample have been collected with the near-infrared integral field spectrograph SINFONI of the VLT under the Large Programme 179.A-0823 (P.I. T. Contini) between April 2007 and January 2011 and including the observations of the pilot runs 75.A-0318 and 78.A-0177. Our subsample of 50 galaxies refers to observations conducted until 2009 and fully reduced and analyzed before 2010.

In the accompanying paper by Contini et al. (2011) the strategy and global physical properties of MASSIV galaxies are detailed, along with a more exhaustive explanation of selection functions. Full details on the data reduction procedures are given in Epinat et al. (2012). Here we provide a short summary.

We used the J- and H-bands to sample the spectral interval $1.08 - 1.41\,\mu m$ and $1.43 - 1.86\,\mu m$ with a spectral resolution of $R \sim 2000$ and ~ 3000, respectively. The majority of our observations were in seeing-limited mode with a $8'' \times 8''$ field-of-view and $0\farcs125 \times 0\farcs25$ pixel scale. For a subsample of seven galaxies we obtained AO observations with a $3\farcs2 \times 3\farcs2$ field-of-view and $0\farcs100 \times 0\farcs050$ pixel scale. To maximize the telescope time, we offsetted the majority of our targets at different positions in the field-of-view of the instrument. This strategy avoids sky frame acquisition (see for details in Contini et al. 2011). In addition, we applied a sub-dithering to place the target at a different position on the chip. Conditions were photometric during the observations with a median seeing of $0\farcs70$ measured on the PSF stars acquired during the night. To accurately point our galaxies, we acquired them through a blind offset from a bright nearby star. We also observed standard stars over the same nights to flux calibrate. Individual exposures range between 300s and 900s with a total on-source integration time that ranges between 1h to 2h.

The core of the data reduction has been performed using the ESO-SINFONI pipeline, version 2.0.0 (Modigliani et al. 2007) complemented with additional routines to homogenize the data processing among the different reducers. We subtract the sky background, skylines, and dark current from the raw science data using the contiguous sky frames obtained with the offset-to-sky sequence. The data were flat-fielded using an internal lamp, wavelength calibrated from the spectra of reference arc-lamps. These processed data frames were then reconstructed into data cubes. Individual cubes of a given observing block were aligned in the spatial direction by relying on the telescope offsets from a nearby bright star and then combined. The rejection of cosmic rays has been applied on the combined cubes. The observations of a telluric standard star of a typically B spectral type follow the science frames and were reduced in a similar way. We extracted the mono-dimensional spectra of the stars by summing the flux of an aperture of diameter of 5 resolution elements to obtain the flux calibration after removing the telluric absorption lines. We corrected for the atmospheric transmission dividing the science cubes by the integrated spectrum of the telluric standard. We created sky cubes to quantify the effective resolution for each

science data cube. The sky cubes were reduced in a similar way as science frames, but no correction for sky subtraction has been applied. We fitted with a Gaussian profile the unblended night sky lines on the extracted, mono-dimensional spectra. The effective FWHM spectral resolution has a typical value of 130 km s^{-1}.

3. Derived quantities

3.1. Morphology and kinematics

We use H$\alpha\lambda$6563Å (and [OIII]λ5007Å line in one case) to derive the dynamical properties. We assume that the ionized gas rotates in a thin disc with a velocity reaching a plateau in the outer regions (but for 8/23 rotating galaxies marked with $^{(c)}$ in column (9) of Tab. 2 this radius is not reached within the area covered by our observations). Using a χ^2 minimization we produce seeing-corrected velocity and dispersion maps of galaxies with geometrical inputs weighted by the SNR of each pixel.

The input geometrical parameters to the fitting model are estimated from the I-band best-seeing CFHTLS[1] Megacam images for all galaxies, but 14^{hr} Wide galaxies that were covered with the I-band CFHT-12K camera only (McCracken et al. 2003). At the typical $z \sim 1.2$ redshift of MASSIV galaxies, I-band images probe the 3200-4200Å rest-frame wavelength range, or U-band. We use the GALFIT software (Peng et al. 2002) that convolves a PSF with a model galaxy image based on the initial fitting parameter estimates with a Sérsic (1968) profile. GALFIT converges into a final set of parameters such as the centre, the position angle, and the axial ratio. Residual maps from the fit were used to optimize the results. The I-band images were also used to calibrate for SINFONI astrometry, in considering the relative position of the PSF star. GALFIT has also been applied on the ionised gas maps (properly deconvolved with a PSF star) in order to derive the semi-major axis disc scale-length. The CFHT images and the kinematic maps are presented in Epinat et al. (2012) where more discussion is presented on the modeling procedure.

The major source of uncertainties in deriving the maximum rotation velocity is the inclination of the studied galaxy. For very small objects the inclination is not robustly constrained, thus for a fraction of galaxies the median inclination value of a randomly distribution of galaxies on the sky (60°) is adopted instead. For this category of objects we have a typical uncertainty of 24° associated to the inclination. Another uncertainty appears when the maximum velocity is not reached within the radius covered by our observations. Other uncertainties entering in the error budget are related to the simplistic disc model adopted. To evaluate the net effects of this assumption would require the assumption of different, detailed modeling schemes, which is beyond the scope of this paper. The final uncertainty associated to our velocities includes both the errors originating from the deprojection of the radial velocity given a certain inclination (estimated with Monte Carlo simulations) and those from the modeling procedure (quantified with simulations on the GHASP local sample following Epinat et al. 2012).

[1] Based on observations obtained with MegaPrime/MegaCam, a joint project of CFHT and CEA/DAPNIA, at the Canada-France-Hawaii Telescope (CFHT) which is operated by the National Research Council (NRC) of Canada, the Institut National des Science de l'Univers of the Centre National de la Recherche Scientifique (CNRS) of France, and the University of Hawaii. This work is based in part on data products produced at TERAPIX and the Canadian Astronomy Data Centre as part of the Canada-France-Hawaii Telescope Legacy Survey, a collaborative project of NRC and CNRS.

3.2. Mass and star formation rate

In this work we obtain the stellar mass from spectral energy distribution (SED) fit to photometric and spectroscopic data with BC03 stellar population synthesis models (Bruzual & Charlot 2003) using the GOSSIP Spectral Energy Distribution tool (Franzetti et al. 2008). We assume a Salpeter initial mass function (Salpeter 1955) with a lower and upper mass cutoff of respectively 0.1 and 100$\mathcal{M}_{\odot}$, a set of delayed exponential star formation histories with galaxy ages in the range from 0.1 to 15 Gyr. As input for the SED fitting we use the multi-band photometric observations available in the VVDS fields, including BVRI data from the CFHT-12K camera, ugriz data from the CFHT Legacy Survey, J and Ks-band data from SOFI at the NTT, from the UKIDSS survey, SWIRE data when available, and the VVDS spectra. Following Walcher et al. (2008) we adopt the probability distribution function to obtain the stellar mass (listed in column (6) of Tab. 2), the absolute magnitude, and the other results of fitting procedure as detailed in Contini et al. (2011).

We estimate the dynamical mass and the gas mass in our galaxies to trace the evolution of both baryonic and dark matter components. As described in the next section our galaxies show a variety of kinematics that we classify in two broad categories: rotators and non-rotating systems (see details in Sect. 3.3 of this paper and in Epinat et al. 2012). The dynamical mass is estimated using the following equation:

$$M_{dyn} = \frac{V^2\,R}{G} + \frac{\sigma^2\,R^3}{G\,h^2} \quad (1)$$

where the first term represents the mass enclosed within the radius R defined as the total extent of the ionized gas, V is the velocity at the same radius, and G is the universal gravitational constant. The second term represents the asymmetric drift correction following Meurer et al. (1996) where σ is the dispersion velocity at R, h is the gas disc scale length in an isotropic geometrical configuration with a surface density described by a Gaussian function. The dynamical mass of each galaxy is given in column (6) of Tab. 2, its error is estimated accounting for the uncertainties related to the inclination and the modeling procedure.

The gas mass is derived with the empirical correlation between star formation rate (SFR) and gas surface density assuming that the gas and the stellar content accounts for the majority of the mass in the inner centre of galaxies. In the local Universe, Kennicutt (1998b) proved that the surface density of gas to star-formation rate follows a power law above some critical gas density (Schmidt 1959, $\Sigma_{SFR} = A\Sigma_{gas}^{n}$) over more than six orders of magnitude in $\Sigma_{\rm SFR}$. This empirical correlation has not yet been routinely proved at high redshift because of the lack of extensive measurements of cold gas mass, but a number of studies on small samples support the validity of this relation at high redshifts (e.g., Erb et al. 2006; Bouché et al. 2007; Daddi et al. 2010; Tacconi et al. 2010). Some detailed studies on individual galaxies also point to a consistency with the local Schmidt law (e.g., the lensed $z = 2.7$ LBG MS1512-cB58, Baker et al. 2004). Thus we compute the star formation rate surface densities using the total SFR and the size of our galaxy.

The SFRs are computed following Kennicutt (1998a). The fluxes are measured on $> 2\sigma$ regions of the flux-calibrated data cubes and corrected for dust reddening using the extinction coefficient derived from the SED fitting (see Contini et al. 2011). The half-light radius, $R_{1/2,gas}$, has been measured as the semi-major axis half-light radius with GALFIT (Peng et al. 2002) on the

Table 2. PROPERTIES OF THE MASSIV SAMPLE

ID (1)	z (2)	*Line* (3)	M_* (4)	M_{gas} (5)	M_{dyn} (6)	R_{last} (7)	$R_{1/2,gas}$ (8)	$R_{1/2,star}$ (9)	V_{max} (10)	V_{max}/σ (11)	Class (12)
020106882	1.3991	Hα	$9.99^{+0.22}_{-0.22}$	9.84	$10.41^{+0.18}_{-0.13}$	5.1	3.79±0.08	3.51± 0.14	133±25	3.2	ROT
020116027	1.5302	Hα	$10.09^{+0.23}_{-0.23}$	9.86	$9.94^{+0.23}_{-0.29}$	6.5	3.56±0.08	4.27± 0.16	27±10	0.6	NON-R
020126402	1.2332[a,b]	[OIII]	$10.09^{+0.26}_{-0.25}$	...	...	...	...	2.12± 0.31	...	...	...
020147106	1.5195	Hα	$10.10^{+0.13}_{-0.13}$	9.89	$11.73^{+0.36}_{-0.36}$	7.8	1.52±0.08	1.17± 0.41	26±51	0.3	ROT[e]
020149061	1.2905	Hα	$10.18^{+0.23}_{-0.23}$	9.89	$11.29^{+0.80}_{-0.80}$	4.8	3.68±0.08	1.09± 0.69	107±210[d]	1.5	ROT
020164388	1.3547	Hα	$10.13^{+0.31}_{-0.31}$	9.83	$10.77^{+0.26}_{-0.33}$	8.2	2.78±2.27	2.72± 0.05	79±19	1.5	NON-R
020167131	1.2246	[OIII][c]	$10.08^{+0.19}_{-0.19}$	9.81	$9.83^{+0.17}_{-0.10}$	1.8	3.96±0.33	2.60± 0.09	127±29	5.0	NON-R
020182331	1.2290	Hα	$10.72^{+0.11}_{-0.11}$	9.92	$10.51^{+0.14}_{-0.13}$	5.5	3.49±2.08	4.19± 0.17	127±25[d]	1.9	NON-R
020193070	1.0279	Hα	$10.15^{+0.20}_{-0.20}$	9.57	$10.14^{+0.11}_{-0.07}$	3.9	4.11±1.37	3.49± 0.09	116±23[d]	3.6	NON-R
020208482	1.0375	Hα[c]	$10.17^{+0.16}_{-0.16}$	8.94	$9.92^{+0.11}_{-0.08}$	1.4	5.50±0.08	3.67± 0.20	158±31	22.9	ROT
020214655	1.0395	Hα	$10.02^{+0.16}_{-0.16}$	9.90	$10.91^{+0.31}_{-0.43}$	5.7	3.23±1.05	1.47± 0.08	52±14	0.8	NON-R
020217890	1.5129[a]	Hα	$10.02^{+0.16}_{-0.16}$	...	...	...	3.57±0.14	...	...	...	
020239133	1.0194	Hα	$9.89^{+0.15}_{-0.15}$	9.49	$10.59^{+0.18}_{-0.17}$	4.8	3.09±0.08	3.14± 0.09	148±33[d]	2.0	ROT
020240675	1.3270	Hα	$9.96^{+0.18}_{-0.18}$	9.50	$10.17^{+0.62}_{-0.62}$	3.8	2.85±0.75	1.09± 0.16	47±92[d]	1.4	NON-R
020255799	1.0351	Hα[c]	$9.87^{+0.16}_{-0.16}$	9.44	$10.37^{+0.36}_{-0.36}$	4.0	2.91±0.08	1.89± 0.26	14±25	0.2	NON-R
020261328	1.5290	Hα	$10.01^{+0.20}_{-0.20}$	9.59	$10.65^{+0.34}_{-0.28}$	5.1	3.22±0.08	1.83± 0.27	120±33[d]	2.2	ROT
020278667	1.0516	Hα[c]	$10.28^{+0.16}_{-0.16}$	9.04	$9.28^{+0.36}_{-0.19}$	1.3	2.35±0.08	2.82± 1.66	76±187[d]	1.5	NON-R
020283083	1.2818	Hα	$10.05^{+0.21}_{-0.21}$	9.52	$9.89^{+0.23}_{-0.21}$	5.6	2.76±0.16	4.29± 0.20	59±12	1.5	NON-R
020283830	1.3949	Hα	$10.37^{+0.17}_{-0.17}$	9.94	$10.81^{+0.03}_{-0.01}$	7.9	3.96±0.33	6.82± 0.16	186±30	11.3	ROT
020294045	1.0028	Hα	$9.80^{+0.15}_{-0.15}$	9.55	$10.93^{+0.21}_{-0.16}$	5.5	3.85±0.16	2.89± 0.10	233±51[d]	3.9	NON-R
020306817	1.2225[a]	[OIII]	$9.76^{+0.20}_{-0.20}$	...	...	...	...	4.22± 0.09	...	...	...
020363717	1.3339	Hα	$9.68^{+0.35}_{-0.20}$	9.90	$11.89^{+0.28}_{-0.28}$	6.0	3.11±0.08	0.72± 0.09	43±85[d]	0.5	NON-R
020370467	1.3338	Hα	$10.57^{+0.14}_{-0.14}$	10.02	$11.22^{+0.00}_{-0.54}$	5.5	3.53±0.08	1.31± 0.25	51±65	0.6	NON-R
020386743	1.0487	Hα	$9.88^{+0.20}_{-0.20}$	9.80	$10.21^{+0.25}_{-0.33}$	5.4	2.99±3.32	2.68± 0.21	41±10[d]	0.8	NON-R
020461235	1.0349	Hα	$10.36^{+0.15}_{-0.15}$	9.40	$9.99^{+0.16}_{-0.10}$	5.4	3.47±0.16	3.96± 0.12	82±16	3.5	ROT
020461893	1.0486	Hα	$9.66^{+0.21}_{-0.21}$	9.54	$10.65^{+0.23}_{-0.31}$	6.5	3.56±0.08	2.66± 0.11	58±13	0.9	ROT[e]
020465775	1.3583	Hα	$10.12^{+0.20}_{-0.20}$	9.99	$10.25^{+0.21}_{-0.25}$	4.9	3.70±0.08	4.04± 0.16	68±15	0.8	NON-R
140083410	0.9435	Hα	$10.07^{+0.18}_{-0.18}$	9.78	$10.62^{+0.35}_{-0.35}$	5.3	3.00±0.08	1.93± 0.19	30±33	0.4	NON-R
140096645	0.9655	Hα	$10.40^{+0.24}_{-0.23}$	10.12	$11.11^{+0.63}_{-0.63}$	4.5	3.41±0.08	1.80± 0.40	295±710	3.9	ROT
140123568	1.0012	Hα[c]	$9.73^{+0.39}_{-0.39}$	9.24	$8.75^{+0.49}_{-0.49}$	0.5	1.44±0.08	1.39± 0.98	50±97[d]	0.7	NON-R
140137235	1.0445	Hα[c]	$10.07^{+0.29}_{-0.29}$	9.77	$8.78^{+0.31}_{-0.10}$	0.7	1.54±1.62	5.45± 2.03	61±11[d]	3.5	ROT
140217425	0.9792	Hα	$10.84^{+0.17}_{-0.17}$	10.45	$11.85^{+0.04}_{-0.02}$	14.5	5.50±0.80	8.96± 0.13	320±46[d]	7.1	ROT
140258511	1.2423	Hα	$11.82^{+0.06}_{-0.09}$	10.21	$10.41^{+0.33}_{-0.33}$	5.2	3.17±0.08	2.62± 2.11	124±26	5.1	ROT
140262766	1.2836	Hα	$9.84^{+0.43}_{-0.43}$	9.38	$10.39^{+0.30}_{-0.30}$	4.1	3.09±0.08	2.07± 0.70	114±226[d]	3.0	ROT
140545062	1.0408	Hα	$10.60^{+0.18}_{-0.18}$	9.61	$11.10^{+0.40}_{-0.40}$	7.5	2.93±0.24	2.89± 6.86	202±45[d]	3.0	ROT
220014252	1.3105	Hα	$10.78^{+0.21}_{-0.21}$	10.42	$11.35^{+0.21}_{-0.26}$	10.3	4.95±0.16	3.32± 0.12	129±27	1.4	ROT
220015726	1.2933	Hα	$10.77^{+0.27}_{-0.27}$	10.09	$10.72^{+0.41}_{-0.20}$	3.7	2.85±0.08	2.76± 0.25	231±354	3.7	ROT
220071601	1.3538[a,b]	Hα	$10.81^{+0.62}_{-0.56}$	...	...	...	...	8.13± 0.13	...	...	...
220148046	2.2442[b]	[OIII][c]	$11.22^{+0.17}_{-0.17}$	10.10	$8.72^{+0.06}_{-0.06}$	0.9	0.82±0.08	1.98± 0.38	61±119	1.3	NON-R
220376206	1.2445	Hα	$10.67^{+0.27}_{-0.26}$	10.51	$11.14^{+0.12}_{-0.11}$	10.0	5.42±0.08	5.29± 0.08	201±27	2.8	ROT
220386469	1.0226[b]	Hα[c]	$10.80^{+0.16}_{-0.16}$	9.64	$9.25^{+0.31}_{-0.32}$	2.6	1.77±0.08	2.90± 0.13	98±20[d]	2.3	NON-R
220397579	1.0379	Hα	$10.23^{+0.17}_{-0.17}$	10.23	$10.97^{+0.23}_{-0.33}$	10.2	3.00±0.07	3.02± 0.32	9±10[d]	0.2	NON-R
220544103	1.3973	Hα	$10.71^{+0.27}_{-0.27}$	10.27	$10.70^{+0.00}_{-0.20}$	7.6	5.31±0.08	5.61± 19.8	137±24	1.9	ROT
220544394	1.0101	Hα	$10.34^{+0.23}_{-0.23}$	9.97	$9.98^{+0.21}_{-0.24}$	5.0	4.49±0.08	3.40± 0.15	55±11	1.1	NON-R
220576226	1.0217	Hα	$10.31^{+0.23}_{-0.23}$	9.97	$10.48^{+0.28}_{-0.28}$	6.1	3.22±0.08	2.16± 0.12	30±12	0.6	NON-R
220578040	1.0462	Hα	$10.72^{+0.17}_{-0.17}$	9.80	$11.05^{+0.41}_{-0.22}$	7.0	6.55±0.08	3.81± 0.12	244±211[d]	4.9	ROT
220584167	1.4655	Hα	$11.21^{+0.24}_{-0.24}$	10.51	$11.28^{+0.07}_{-0.05}$	13.1	5.24±0.08	7.17± 0.19	235±35	4.8	ROT
220596913	1.2658[b]	Hα	$10.68^{+0.30}_{-0.30}$	9.53	$10.66^{+0.04}_{-0.04}$	9.3	5.09±0.08	9.49± 11.5	141±10	3.7	ROT
910193711	1.5564[b]	Hα	$9.99^{+0.42}_{-0.18}$	10.14	$10.39^{+0.31}_{-0.44}$	4.1	1.61±0.08	2.27± 0.06	63±12	0.8	NON-R
910279515	1.4013[b]	Hα[c]	$10.79^{+0.14}_{-0.14}$	9.71	$10.34^{+0.07}_{-0.05}$	2.7	4.05±0.25	4.44± 0.11	265±18	5.6	ROT

Tab. 2. (1) VVDS identification number. (2) Redshift derived from SINFONI observations of the emission line (H$\alpha\lambda$6563Å or [OIII]λ5007Å) tabulated in column (3). (4) Stellar mass in solar mass units. (5) Gas mass derived using the Kennicutt-Schmidt formulation (Kennicutt 1998b). (6) Dynamical mass computed following Eq. 1 and based on the best-fitting parameters of the kinematic model. (7) The radius computed as the total size of the ionized emission map with a confidence level larger than 2σ. (8) The gas half-light radius estimated on the SINFONI maps of the lines tabulated in column (3). (9) The observed I-band half-light radius. (10) Maximum velocity deduced from model fitting. (11) Ratio of the maximum rotation velocity over the velocity dispersion. (12) Kinematic classification (R: Rotating objects, NON-R: non-rotating systems). [a] This redshift is computed on the original VIMOS spectrum. [b] Observations with Adaptive Optics. [c] Galaxy with low signal-to-noise ratio ($3 \leq SNR \leq 4.5$) plotted with empty symbols in the figures. Galactic properties of SINFONI observations with a signal-to-noise ratio below 3 are not reported. [d] Galaxy for which the plateau velocity has not been reached. [e] Galaxy for which the criterion on $v/\sigma > 1$ is not fulfilled, thus not included in the purely rotating disc sample. The public access to data is at http://cosmosdb.iasf-milano.inaf.it/VVDS-SINFONI.

spatial extent of the ionized gas (H$\alpha\lambda$6563Å or [OIII]λ5007Å) emission, after convolving with the PSF of a bright star nearest in time to the scientific observations. Maps of the residuals were used to optimize the results. Assuming the Schmidt law holds in our redshift interval we estimate the gas mass M_{gas} using the relation between the gas density Σ_{gas} and the star-formation rate surface density Σ_{SFR} (Kennicutt 1998b):

$$\frac{\Sigma_{SFR}}{M_\odot\ yr^{-1}\ kpc^{-2}} = 2.5\times10^{-4}\left(\frac{\Sigma_{gas}}{M_\odot pc^{-2}}\right)^{1.4} \quad (2)$$

where the relation between the observed Hα luminosity per unit area, or the Hα surface density $\Sigma_{H\alpha}$, and the gas surface density is:

$$\frac{\Sigma_{gas}}{M_\odot\ pc^{-2}} = 1.6\times10^{-27}\left(\frac{\Sigma_{H\alpha}}{erg\ s^{-1}\ kpc^{-2}}\right)^{0.71}. \quad (3)$$

The mass of the gas associated with the measured star formation is given by:

$$M_{gas} = \Sigma_{gas}\times Area \quad (4)$$

where the *Area* in Eq. 4 is the total spatial extent of the ionized gas measured on $> 2\sigma$ regions of the flux-calibrated data cubes.

The gaseous masses are given in Tab. 2, the associated error is analytically propagated from the errors in the observations using conventional techniques. Further details on the error analysis are described in the accompanied paper (Epinat et al. 2012). Typical value of the error is of the order of 0.25 dex. We note that different calibrations exist for the Kennicutt-Schmidt law at higher redshift, e.g., Bouché et al. (2007) suggest a steeper power-law index (1.7 instead of 1.4 in Eq. 3) for $z > 2.5$ starburst galaxies. This steeper formulation implies a < 0.3 dex difference in the gas computation. Given the uncertainties involved in deriving this quantity, a different value for the slope does not have any significant impact on our data interpretations (see Gnerucci et al. 2011).

3.3. Kinematic classification

To classify our sample we adopt a kinematic classification that relies on a combination of observed galaxy properties. We refer to Epinat et al. (2012) for a full description of the methodology for which we provide here a brief outline. In a first step eight of us classified independently all the sample using personal criteria. Subsequently we reconciled the criteria into a new agreed scheme: we assign to each galaxy a confidence flag generated by the concordance among the classifiers.

When galaxies satisfy all the following conditions they are kinematically flagged as:

Rotating discs: when the velocity field is well described by a symmetrically rotating disc with a kinematic position angle that does not differ significantly from the morphologically derived major axis. We quantify these conditions assuming that the mismatch between the position angles is lower than ±20° and that the residuals of the modelled velocity field over the measured velocities are less than a certain fraction (< 20%). In this work we also require that galaxies classified as "rotators" are rotationally supported imposing that the rotation velocity must be larger than the dispersion velocity (i.e., $v/\sigma > 1$ as listed in column (12) of Tab. 2.)

or

Non-Rotating systems: At least one of the conditions on the residuals, position angles, or rotation-over-chaotic motions is violated. In this class fall galaxies with some kind of anomalies in the velocity field, merger-like systems, and/or objects with off-peaked distributions of the dispersion velocity, but also possibly slow rotators or face-on systems with the observed velocity gradient lower than typically $\pm25 km\,s^{-1}$.

4. The gas properties in MASSIV star-forming galaxies

We compare the total extent of the ionized gas, R_{last}, with the half-light radius of the stellar component, $R_{1/2,star}$, for the class of rotating and non-rotating disc galaxies in Fig. 1 (in the top panel with blue colour-coded circles and in the bottom panel with red colour-coded squares, respectively). R_{last} is the radius computed as the total size of the ionized emission map that has a confidence level larger than 2σ. The half-light radius of stars is measured on the observed I-band images, or rest-frame U-band wavelengths. The error bars in Fig. 1 are the 1σ uncertainties derived from the GALFIT procedure on the images corrected for their respective PSF FWHM. The histograms show the distributions of the gas and stellar radii of the classes. The solid line is the linear fit[2] to the data and the dashed line shows the standard deviation.

The dotted line is the correlation observed in a thin exponential disc between the radius of the total ionized gas emission and the half-light radius of the stellar component, $R_{last} \sim 1.9\times R_{1/2,star}$. Assuming that the optical radius equals 3.2 times the disc scalelength following Persic & Salucci (1991), the half-light radius is 1.678 times the disc scale length. The total ionized gas, R_{last}, is close to the optical radius as in local star-forming galaxies (e.g., Garrido et al. 2005).

For the class of rotators we obtain median values of $R_{last} = 5.40^{7.60}_{4.80}$ kpc and $R_{1/2,star} = 3.51^{5.29}_{2.62}$ kpc, and for non-rotators $R_{last} = 5.50^{6.50}_{4.00}$ kpc and $R_{1/2,star} = 2.68^{3.40}_{1.47}$ kpc (with the extremes representing the quartiles of the distribution for the two classes). Non-rotating galaxies are more compact in the extent of the stellar component than rotators, but similar in the gas extent. For rotating galaxies we obtain that $R_{last} = 1.63\pm0.14\times R_{1/2,star}$ with an intrinsic scatter of $\sigma_{intr} = 2.23$ (and total scatter of $\sigma_{tot} = 2.70$). The same correlation for non-rotating systems is $R_{last} = 1.70\pm0.21\times R_{1/2,star}$ ($\sigma_{intr} = 2.20$ and $\sigma_{tot} = 2.66$). In the local Universe the extent of the ionized gas component in star-forming galaxies is close to the optical radius (e.g., Garrido et al. 2005). Within 1σ dispersion, and considering the associated uncertainties, all MASSIV rotating galaxies are within the expected statistical trend found by Persic & Salucci (1991). A similar agreement has been found by Puech et al. (2010) for their IMAGES sample at $z \sim 0.6$. Similarly to Puech et al. (2010) and Bamford et al. (2007), we notice a fraction of non-rotating galaxies with a larger gaseous extent than their stellar counterpart exceeding the predicted correlation by 1σ. While in the sample of Puech et al. (2010) the cases where this correlation

[2] We fit a linear relationship to the data using the MPFITEXY routines (Williams et al. 2010). The MPFITEXY routine depends on the MPFIT package (Markwardt 2009). This routine properly adjusts the intrinsic scatter to ensure the minimisation of chi-square with an iterative prescription.

is not respected are the ones with the UV light extending further out the field-of-view of the FLAMES/IFU (3″ × 2″), in the MASSIV sample the two outliers show a signature of a close companion, one of which is detected in Hα.

We will further investigate these trends and their relation with the environment at the completion of the survey when we will develop a classification scheme enabling us to distinguish the various mechanisms of disturbance in inclined and face-on galaxies as well as in compact and dispersion-dominated spheroids. For simplicity, at the present time we flag all these galaxies in a unique class named non-rotators (plotted with red-coded, square symbols in all figures).

We now compare our measurements with the characteristic sizes of galaxies as found by other similar surveys to analyse the correlation among properties like stellar mass, size, and velocity. In IMAGES (Puech et al. 2010) the total light radius measured on the ionized [OII] gas of rotating galaxies has a median of 11.29 kpc and ranges from 8.25 kpc (first quartile, or 25th percentile of distribution) to 11.99 kpc (last quartile, or 75th percentile). The median value of the half-light rest-frame UV radius is 6.27 kpc with 4.26 kpc and 6.53 kpc as quartiles of the distribution. We note that the IMAGES disc size is the maximum between the total size measured on the ionized [OII] gas and the half-light rest-frame UV light multiplied by 1.9. In SINS (Cresci et al. 2009), the half-width half-maximum size (HWHM) measured on the ionized Hα maps is interpreted as exponential disc scale-lengths of $z \sim 2$ rotating SINS discs, and ranges from 4.11 kpc to 6.35 kpc with median of 5.87 kpc. The circular half-light sizes of the total SINS $z > 2$ sample computed on Hα maps by Förster Schreiber et al. (2009) is in the range 2.40 – 4.60 kpc and has a median value of 3.10 kpc. Dutton et al. (2011) claim for a fundamental disagreement of the SINS HWHM sizes derived by Cresci et al. (2009) and the SINS half-light radii by Förster Schreiber et al. (2009), as already noted by these latter authors who reject the possibility to attribute the discrepancy to non-exponential discs. At higher redshift the AMAZE/LSD sample of Gnerucci et al. (2011) is constituted by eleven $z \sim 3$ rotating galaxies. The characteristic radius of these exponential discs measured on Hα maps ranges between 0.71 kpc and 1.73 kpc (first and last quartile of the distribution) with a median value of 1.24 kpc. Overall, comparing directly to the values of Puech et al. (2010) as we adopt the same radius definition, we find that IMAGES radii are a factor of 1.5 larger than MASSIV radii. Instead, compared to those of SINS by Förster Schreiber et al. (2009), we find similar sizes (our half-light sizes measured on Hα maps are in the interval $R_{1/2,gas} = 2.85 - 3.96$ kpc with a median of 3.47 kpc). Both SINS and MASSIV radii are approximately three times larger than sizes sampled at $z \sim 3$ in AMAZE/LSD by Gnerucci et al. (2011).

We investigate further the disc properties to verify the hypothesis whether our MASSIV discs have exponential profiles. Discs of ionized gas have frequently an irregular, clumpy distribution as it is also reported for SINS galaxies. Despite the simplistic assumption both the Sérsic index distribution and the correlation between exponential and half-light radii suggest that MASSIV discs can be approximated to exponential discs. The same qualitative conclusion has been reported for SINS discs (Förster Schreiber et al. 2009).

In summary, our resulting characteristic size agrees within the statistical correlations previously assessed in the literature. The radius taken to derive the velocity is critical to avoid the insertion of systematic biases (see Noordermeer & Verheijen 2007). The relation obtained between the size of the stars and that of the gaseous component ensures that this latter physical quantity is reliable for the determination of the maximum velocity.

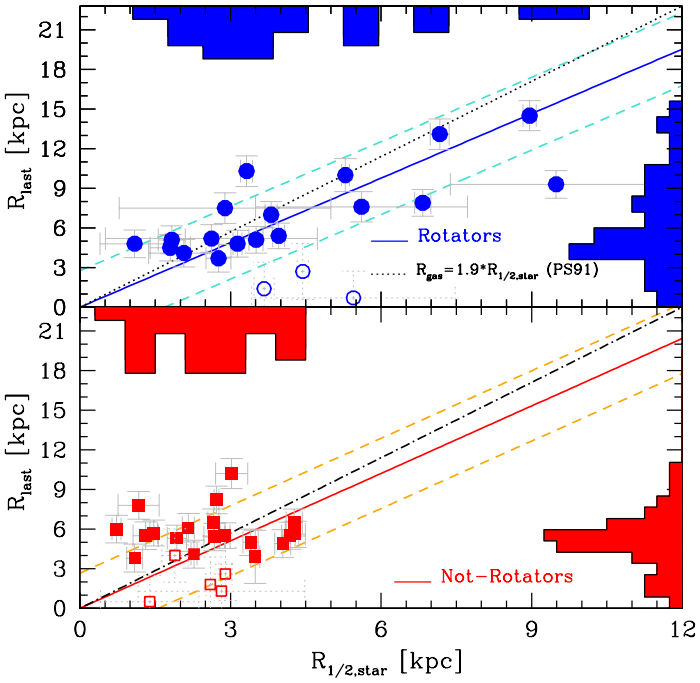

Fig. 1. Comparison between R_{last} and $R_{1/2,star}$ radii computed as the size of our ionized gas maps with a confidence level larger than 2σ and the half-light radius of the stellar continuum measured on the observed I-band best-seeing CFHTLS images, respectively. Within the errors both rotators (top panel, blue circle) and non-rotators (bottom panel, red square) agree with the expected statistical trend $R_{last} = 1.9 \times R_{1/2,star}$ found by Persic & Salucci (1991, PS91) plotted with a black dotted line. The blue/red solid lines are the best-fit to the rotators/non-rotating galaxies (dashed lines show the total scatter of the correlations). The empty, dashed symbols show galaxies detected with a low signal-to-noise ratio ($3 \leq SNR \leq 4.5$).

Figure 2 shows the stellar mass of MASSIV galaxies versus the dynamical (top panel) and gas (bottom panel) mass. The methods used to derive these masses are described in Sect. 3.2. The total distributions of these quantities are shown as full gray-coded histograms while those with blue, positive-oblique angle (or red negative-oblique angle) refer to rotating (non-rotating) galaxies. Dynamical masses range between 2.57×10^{10} $\mathcal{M}_{\odot}$ and 1.29×10^{11} $\mathcal{M}_{\odot}$ with a median value of 5.01×10^{10} $\mathcal{M}_{\odot}$ for the class of rotating galaxies (dashed-point horizontal line in the bottom panel of Fig. 2), and $0.95 - 8.13 \times 10^{10}$ $\mathcal{M}_{\odot}$ with a median value of 2.45×10^{10} $\mathcal{M}_{\odot}$ for non-rotating galaxies (dashed horizontal line). We estimate a gaseous mass in the interval between 3.38×10^{9} $\mathcal{M}_{\odot}$ (first quartile) and 1.64×10^{10} $\mathcal{M}_{\odot}$ (last quartile) with a median value of 7.85×10^{9} $\mathcal{M}_{\odot}$, and stellar masses in the following range $1.48 - 5.87 \times 10^{10}$ $\mathcal{M}_{\odot}$ with a median value of 3.98×10^{10} $\mathcal{M}_{\odot}$ in rotating galaxies. Median values for non-rotators are $M_{star} = 1.23 \times 10^{10}$ $\mathcal{M}_{\odot}$ and $M_{gas} = 6.71 \times 10^{9}$ $\mathcal{M}_{\odot}$ with ranges between $\Delta M_{star} = 0.90 - 1.90 \times 10^{10}$ $\mathcal{M}_{\odot}$ and $\Delta M_{gas} = 3.51 - 9.37 \times 10^{9}$ $\mathcal{M}_{\odot}$.

Within their uncertainties only few galaxies lie in the forbidden region of $M_{star} > M_{dyn}$. The only strongly deviating rotating galaxy (empty, dashed symbol) has been detected with a low

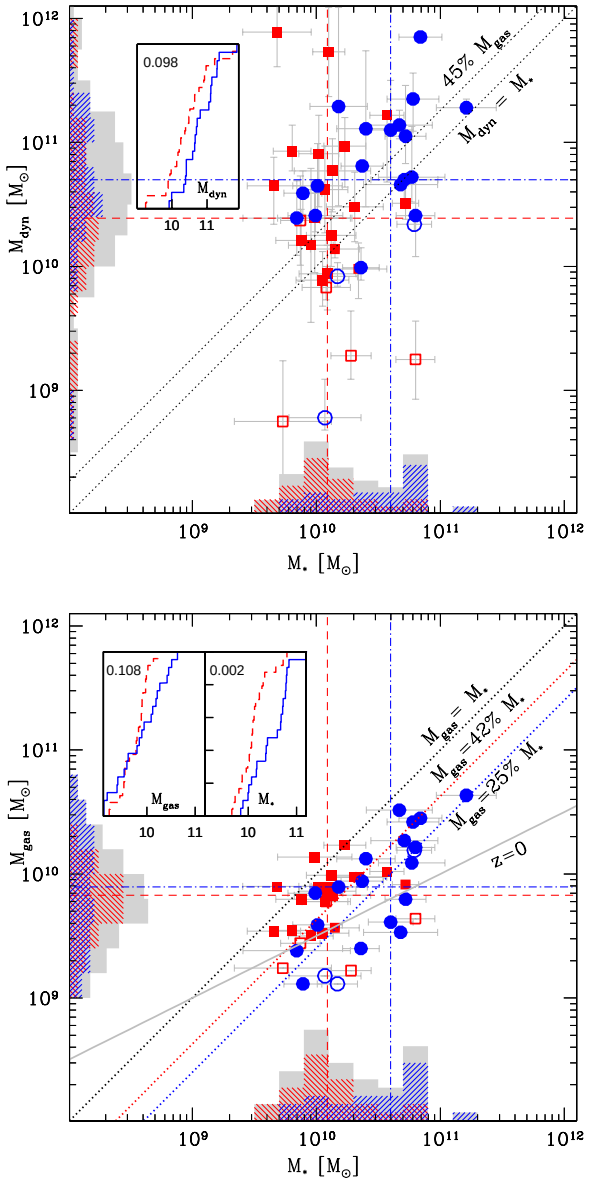

Fig. 2. The stellar mass content of MASSIV galaxies compared to the dynamical mass derived from the dynamical modeling (top panel) and to the gas content derived using the Kennicutt-Schmidt formulation (bottom panel). Symbols are as in Fig. 1. The horizontal and vertical histograms represent the distribution of the stellar and dynamical masses (top) and gas mass (bottom panel). The horizontal and vertical lines are the median values of rotators (point-dashed blue line) and non-rotators (dashed red line), respectively. Dashed diagonal lines in the bottom panel show the condition: $M_{gas} = frac \times M_{star}$ where $frac$ is equal to 25% for rotating galaxies and 42% for non-rotators (or 20% and 30% of the baryonic mass, respectively). The solid line is the local relation proposed by Schiminovich (2008) using the GALEX Arecibo SDSS survey of cold HI gas. In the inserted panels the cumulative distributions for stellar-, dynamical-, and gas-mass are plotted for rotators (solid, blue line) and non-rotators (dashed, red line) along with the probability for the two classes to be statistically different.

signal-to-noise (∼ 3.5). We have a probability of $P = 7.5 \times 10^{-2}$ and $P = 1.5 \times 10^{-4}$ that the stellar mass is uncorrelated to dynamical and gas mass using the Spearman correlation test. The correlation is statistically significant in particular for the stellar and gas masses. In the inserted panels of Fig. 2 we show the cumulative distributions of these quantities for rotators (solid, blue line) and non-rotators (dashed, red line) along with the probability for the two classes to be statistically different using the Kolmogorov-Smirnov test.

We assume no contribution from dark matter in the inner centre of galaxies. It is the best hypothesis to assume given the inability to measure the dark matter distribution in high−z galaxies. This hypothesis has been adopted in earlier studies, e.g., by Gnerucci et al. (2011). With this assumption the mass in gas taken as difference between dynamical and stellar mass of both classes of rotator and non-rotator galaxies, is on average a fraction of ∼ 45% of the dynamical mass (diagonal dotted line), and approximately 20% of the stellar mass or 17% of the baryonic mass. A consistency picture is obtained for rotating galaxies when deriving the gas mass from the Kennicutt-Schmidt law. We fit a content of gas that is 25% of the stellar mass (or 20% of the baryonic mass) in rotating galaxies with typical errors associated to the fit of the order of 5 − 6%.

The gas content in non-rotating galaxies is definitively higher (∼ 42% of the stellar mass, or 30% of the baryonic mass) when using the Kennicutt-Schmidt law. Taking into account that this class of galaxies may contain face-on discs, this fraction represents a lower limit. The same value derived as difference between dynamical and stellar mass is somehow lower. It can be justified by two factors: 1) the inclusion of merging systems in the class of non-rotating galaxies that may have not yet exhausted their gas reservoir; 2) the different properties of dark matter halos in rotators and spheroidal galaxies. In nearby galaxies, within the optical radius the dark matter content is suspected to be higher in rotators than in spheroids (Persic et al. 1996). Thus for the same dynamical mass, the fraction of gas and stars should be lower in rotators than in our class of non-rotating systems.

If we fix the slope to the local relation proposed by Schiminovich (2008) using the GALEX Arecibo SDSS survey of cold HI gas, we obtain a weak evolution of +0.17 dex to $z = 1.2$ for the entire sample (or +0.11 dex for rotators and +0.21 dex for non-rotating galaxies). We emphasize that the selection criteria adopted to build up the MASSIV sample lead to a subsample of non-rotating galaxies with a lower content of stellar mass at fixed gas and dynamical mass.

The fraction of gas in $z \sim 0.6$ IMAGES galaxies ranges between 30% as derived from the evolution of the gas-metallicity relation (Rodrigues et al. 2008) and 45% of the stellar mass obtained with the inverse Kennicutt-Schmidt law by Puech et al. (2010). The gas fraction quoted by Cresci et al. (2009) for SINS galaxies at $z \sim 2$ is in the interval 23 − 30% of the dynamical mass, but including a dark matter contribution of 40%. At higher redshift ($z > 3$, the AMAZE/LSD surveys) these values are too uncertain (Gnerucci et al. 2011).

Based on direct estimates using molecular observations (e.g., Daddi et al. 2010; Tacconi et al. 2010), the gas mass in disc galaxies ranging in the interval between 34-44% of the baryonic mass, is slowly decreasing in the last 8-10 Gyr. Our results are in full agreement with a slow decrease of the gas mass content in disc galaxies since $z \sim 1.2$ with a gas fraction that halves progressively down to the local Universe.

5. The size - mass - velocity relation

In this section we examine the fundamental relations existing in the MASSIV sample at $1.0 < z < 1.6$. We compare their sizes, stellar masses, and rotation velocities to galaxy samples available in the literature at different redshifts to investigate the evolution of these properties. In particular, we derive the relation between the luminosity (or stellar mass) and rotational velocity as introduced by Tully & Fisher (1977), or Tully-Fisher relation (TFR). We further explore the shift in the zero point of this relation and the other fundamental relations that unveil the inter-connection between dark and luminous matter for galaxies at different cosmic epochs.

5.1. The size - mass relation

The evolution of the size - stellar mass relation in rotating galaxies at $1.0 < z < 1.6$ is shown in the top panel of Fig. 3. The distribution of the MASSIV rotating galaxies in this plot (blue-coded circles) is consistent with a mild dependence between the disc size and the stellar mass. Taking into account the relatively limited statistics associated to a disc size representing only a lower limit (as measured on galaxies with a signal-to-noise ratio above 3), we interpret this plot in the frame of its evolution to the local relation fixing the slope to the local relation as derived by Dutton et al. (2011). This relation is based on the local I-band disc scalelength - stellar mass relation from Dutton et al. (2007) with stellar masses from Bell et al. (2003) and Bell & de Jong (2001). The evolution of the relation is only slightly stronger using the V-band instead of the I-band size-stellar mass relation derived from the SDSS data. This radius is scaled to the half-light radius which is 1.678 times the scale length for the exponential profile. This local relation is plotted in Fig. 3 as dashed, black line. The solid, blue line is the fit to the MASSIV rotating galaxies. To make a consistent comparison to our measurements we plot in this figure only the evolution reported in those studies using the sizes measured on the ionized gas (Hα, or [OII]) maps. The best fit obtained using SINS galactic sizes defined as the HWHM Hα radii (Bouché et al. 2007; Cresci et al. 2009) is plotted with a dotted-dashed, orange line and with long-dashed, orange line when the size is defined as the half-light Hα radius by Förster Schreiber et al. (2009). Note that difference in the evolution of this relation is due to the method used to measure the disc sizes by Bouché et al. (2007); Cresci et al. (2009) and by Förster Schreiber et al. (2009) (cf. Dutton et al. 2011). We plot with a dotted, red line the evolution measured on IMAGES rotating galaxies using as disc size the maximum between the total size measured on the ionized [OII] gas and the half-light rest-frame UV light multiplied by 1.9. All quantities are consistently rescaled to our Salpeter IMF.

There is a general consensus on the mild evolution of the disc size in star-forming galaxies up to $z \sim 1$ (for example as measured by Williams et al. (2010) taking the circularized rest-frame I-band half-light radii of disc-dominated galaxies, and by Trujillo et al. (2006) taking the circularized rest-frame V-band half-light radius). Compared to the present-day disc sizes, the $z = 1$ counterparts are *smaller* by ∼ 0.10 dex at fixed stellar mass and rotation velocity (e.g., Dutton et al. 2011). This picture agrees well with the theoretical predictions (Blumenthal et al. 1984; Dalcanton et al. 1997; Mo et al. 1998; Firmani & Avila-Reese 2000; de Jong & Lacey 2000; Pizagno et al. 2005; Dutton et al. 2007).

At $z \sim 1.2$ we report an evolution size−stellar mass relation of −0.14 dex using the half-light Hα radius that is quite similar to earlier findings at $z \sim 1$. Above $z \sim 1$ the evolution of disc sizes in literature is less clear, even with opposite trends. Trujillo et al. (2006) found a factor of two smaller half-light sizes at $z \simeq 2.5$ at fixed stellar mass relative to $z = 0$ galaxies. A similar evolution is reported by Williams et al. (2010) in star-forming galaxies at $z = 2$. The evolution of circular half-light Hα sizes as measured by Förster Schreiber et al. (2009) and reported by Dutton et al. (2011) on SINS data at similar redshifts is smaller than previously quoted results, i.e., -0.07 ± 0.05 dex to be compared with −0.28 dex by Trujillo et al. (2006). This discrepancy is attributed by Dutton et al. (2011) to the difference in the half-light radius measured on the Hα maps and rest-frame optical band images. Taking into account this difference their results can be reconciled. A different trend is obtained using measurements of Cresci et al. (2009) on the same SINS data by Dutton et al. (2011). Using the half-width half-maximum size interpreted as exponential disc scale-lengths, SINS disc galaxies presented in Cresci et al. (2009) are ∼ 1.6 times *larger* at $z = 2$ than their local counterparts at fixed stellar mass. Even if a factor of −0.07 dex caused by the skewed distribution towards low inclinations reduces the discrepancy, the values remain significantly inconsistent by a factor of three with the measurements of Trujillo et al. (2006) and Williams et al. (2010) (cf. Dutton et al. 2011). This discrepancy between data-sets increases at higher redshifts if we explore the AMAZE/LSD sample by Gnerucci et

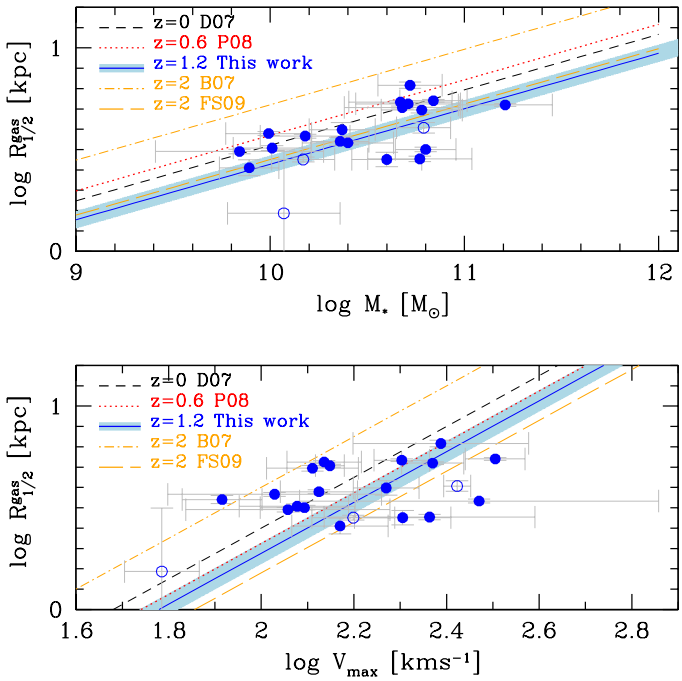

Fig. 3. The stellar mass−size relation (**top panel**) and the velocity−size relation (**bottom panel**) for MASSIV rotating galaxies at $z \sim 1.2$ (solid, blue line with the 1σ error of the correlation illustrated by the light blue area). The local relation by Dutton et al. (2007, D07) is shown as short-dashed, black line. We overplot the best fit relations obtained by Puech et al. (2008) (P08, $z \sim 0.6$, dotted red line), by Bouché et al. (2007) and Cresci et al. (2009) at $z \sim 2$ (B07, dotted-dashed orange line), and by Dutton et al. (2011) using measurements by Förster Schreiber et al. (2009) (FS09, $z \sim 2$, long-dashed orange line). The symbols are as in Fig. 1.

al. (2011). The sizes of the discs are more than four times *higher* in the past than in their local counterparts. We can cautiously speculate that this strong evolution may be caused by a selection effect in the AMAZE/LSD galaxies and the difficulties in measuring realistically the Hα sizes at such high redshifts ($z \sim 3$).

Comparing the evolution computed directly from the half-light radii measured in Hα, we obtain at $z \sim 1.2$ the similar evolution as derived from SINS data at $z \sim 2$ by Dutton et al. (2011), based on measurements by Förster Schreiber et al. (2009). However if we account for the shift suggested by Dutton et al. (2011) that converts our Hα sizes at $z \sim 1.2$ to their optical band half-light radii, we should have a stronger evolution with redshift, i.e., -0.21 dex instead of -0.09 ± 0.04. Conversely, we do not find the same conversion as suggested by Dutton et al. (2011) in the ratio of galaxy sizes (e.g., between our observed I-band and Hα). Furthermore, our results on the evolution of the disc size is perfectly in agreement with the evolution up to $z \sim 1$ found by Williams et al. (2010) and Trujillo et al. (2006), especially taking into account the associated uncertainties on the measurements and the adopted assumptions. Therefore based on the current data-set we suggest a mild evolution in the size - stellar mass relation of rotating galaxies at $z \sim 1.2$. An homogeneous comparison of MASSIV galaxies at $z \sim 2$ and $z \sim 1$ that will be possible at the completion of this survey, will provide a definitive answer to this controversial issue.

5.2. The size - velocity relation

The bottom panel of Fig. 3 shows the relation between the disc scale length and the maximum rotation velocity for MASSIV rotating galaxies and for samples from the literature at different redshifts.

The distribution of the MASSIV rotators in this plot (blue-coded circles) is consistent with no dependence between the disc size and the stellar mass. For the reasons explained in Sect. 5.1, we discuss hereafter the size-velocity relation using the slope determined for local galaxies. We observe a shift of -0.12 ± 0.05 dex of the relation at $z \sim 1.2$ with respect to the local I-band size-velocity distribution computed by Dutton et al. (2007). As reported by Puech et al. (2007) different calibrations proposed to describe this correlation show very similar results, despite the different quantities used to trace the galactic properties. Puech et al. (2007) found some IMAGES rotating galaxies at $z \sim 0.6$ with a relatively lower disc scale length at fixed velocity compared to local rotators (cf. blue circles in their Fig. 3), although the majority of them lies on the distribution of local rotating discs. We fit their rotating galaxies with a relation showing a marginal evolution of -0.08 ± 0.06 from $z \sim 0.6$ to $z \sim 0$.

At $z \sim 2$ the results differ with authors. A consistent evolution with our measurements is observed at higher redshift adopting the half-light sizes as computed by Förster Schreiber et al. (2009). The evolution at $z \sim 2$ shows evenly smaller sizes at a given maximum rotation velocity relative to lower redshift galaxies with an offset of -0.22 ± 0.06 dex from $z = 2$ to $z = 0$ (cf. Dutton et al. 2011), and -0.10 dex to $z \sim 1.2$. At $z \sim 2$ a different trend is observed by Bouché et al. (2007) combining data from the SINS survey (Cresci et al. 2009) and from Courteau (1997) at $z = 0$. Bouché et al. (2007) found no evolution of the zero-point of the size-velocity relation from $z = 2$ to $z = 0$. Dutton et al. (2011) attribute this discrepant result to an inconsistency in the SINS half-width half-maximum size reported in Cresci et al. (2009) and interpreted as exponential disc scale-lengths.

The size-velocity relation shows at all cosmic times a large scatter (of the order of ~ 0.2 dex). The scatter reported in previ-

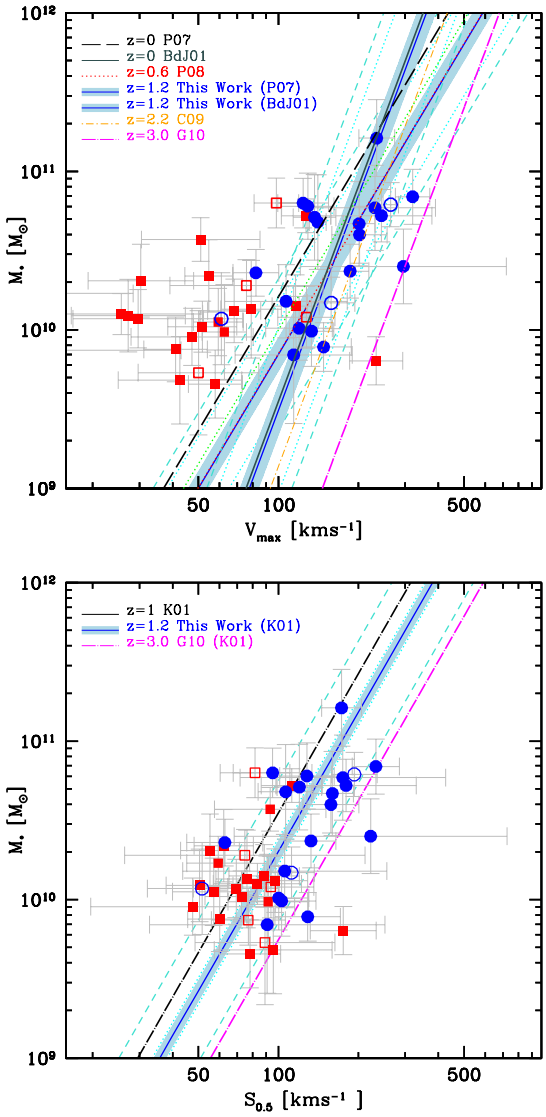

Fig. 4. (**Top**) The stellar mass TF (smTF) relation at $z \sim 1.2$ based on the MASSIV rotating galaxies. Symbols are as in Fig. 1. Errors on the velocities are computed using GHASP simulations to account for various uncertainties. The smTF for the MASSIV rotators is calibrated using either the local slope defined by Pizagno et al. (2007, P07) or by Bell & de Jong (2001, BdJ01) (dashed black line and solid black line, respectively). The solid-blue lines are the best-fit to MASSIV rotating galaxies and the cyan shaded area shows the 1σ error on the zero-point parameter (the intrinsic and total scatter is plotted as cyan dotted line and cyan dashed line, respectively). Other fits are by Puech et al. (2008) (P08, $z \sim 0.6$, dotted red line), Cresci et al. (2009) (C09, $z \sim 2.2$, short-dashed-dotted orange line), and Gnerucci et al. (2011) (G11, $z \sim 3$, long-dashed-dotted magenta line). (**Bottom**) The relation between the stellar mass and the contribution of both ordered and chaotic motions ($S_{05} = \sqrt{(0.5 \times v_{rot}^2 + \sigma_0^2)}$, Kassin et al. 2001, K01) is shown. The cyan shaded area shows the 1σ error on the zero-point parameter, the cyan dotted line and cyan dashed line are the intrinsic and total scatter, respectively. We overplot the best-fit relation by Kassin et al. (2007) at $z \sim 1$ (K01, dot-dashed black line) and by Gnerucci et al. (2011) at $z \sim 3$ (G11, dot-dashed magenta line). Symbols are as in Fig. 1.

ous analyses at high-z are likely due to the difficulties in discerning kinematically complex systems, that translate in uncertainties in the estimation of the characteristic radius of the system. While we are not immune to this subtle possibility, the statistical trend observed between the size of our ionized emission maps and our radius of the stellar continuum on the broad-band images of rotating galaxies, ensures reliable quantities. The local relations studied by e.g., Courteau (1997) and Mathewson et al. (1992) and better constrained in that respect, also show a large scatter of this relation suggesting a physical meaning of this dispersion.

5.3. The mass - velocity relation

In the top panel of Fig. 4 we show the correlation between the stellar mass and the rotation velocity at $z \sim 1.2$ of the MASSIV galaxies. Rotating galaxies are plotted with blue-coded circles. They are the sole class of galaxies included in our best fitting procedure. We plot non-rotating galaxies with red-coded, square symbols. The errors on the velocities are computed using simulations on a local sample to account for various uncertainties (see for details Epinat et al. 2008). The errors on the stellar mass are described in Contini et al. (2011). Consistent to what has been done in the previous section, given the relatively limited statistics at this stage of the survey we set the slope to the local calibration. To make a fair comparison with the published data at different redshifts, and to allow for future comparisons, we fit our data with the two most widely used calibrations. In particular, we calibrate the stellar mass TF relation (smTFR) with the local slope by Pizagno et al. (2007) to compare with the IMAGES sample at $z \sim 0.6$ by Puech et al. (2008, 2010). The local calibration by Pizagno et al. (2007) based on a representative galaxy subsample extracted from the SDSS and revised by Hammer et al. (2007) is plotted in Fig. 4 with dashed, black line. The best fit by Puech et al. (2008) is plotted with a dotted red line. We calibrate the relation with the local slope defined by Bell & de Jong (2001) to compare with the SINS sample at $z \sim 2.2$ by Cresci et al. (2009) and with the LSD/AMAZE galaxies at $z \sim 3$ by Gnerucci et al. (2011). The local calibration by Bell & de Jong (2001) is plotted in Fig. 4 with a solid, black line. The best fit by Cresci et al. (2009) is shown with a short-dashed-dotted orange line and that by Gnerucci et al. (2011) with a long-dashed-dotted magenta line. The Bell & de Jong (2001) calibration is based on the local sample by Verheijen (2001) who selected predominantly low-mass, gas-rich galaxies observed with the 21cm HI emission (Puech et al. 2010; Hammer et al. 2007). The resulting relation is steeper than Pizagno et al. (2007) reference. The two relations start to be equivalent around a velocity of ~ 200 km s^{-1} and a stellar mass of $\sim 10^{11}$ $\mathcal{M}_{\odot}$, thus samples with these galactic properties are not substantially affected by the choice of the calibration. The vast majority of our MASSIV galaxies are located below these values. In consequence, adopting one, or the other calibration affects the strength of the evolution in the velocity-mass relation. We compute for each calibration the zero-point of the correlation, its error, its intrinsic and total scatter. All the above-mentioned studies have been opportunely rescaled to account for our Salpeter IMF.

For rotators we obtain an evolution from $z = 0$ in stellar mass of the smTFR zero point of -0.36 ± 0.11 dex, using as reference the SDSS subsample by Pizagno et al. (2007) (with an intrinsic scatter of $\sigma_{intr} = 0.32$ dex and a total scatter of $\sigma_{tot} = 0.48$ dex). Instead, using the Bell & de Jong (2001) calibration we obtain a zero-point at $z \sim 1.2$ that is consistent with no evolution since $z \sim 0$ (or -0.05 ± 0.16 dex, $\sigma_{intr} = 0.52$ and $\sigma_{tot} = 0.72$). The solid, blue lines are the best-fit to MASSIV rotators and the cyan shaded area shows the 1σ error on the zero-point parameter (the intrinsic and total scatter is plotted as cyan dotted and cyan dashed line, respectively).

The shift in the zero point of the smTFR with respect to $z = 0$ computed by Puech et al. (2008, 2010) at $z \sim 0.6$ is surprisingly high (-0.34 dex in stellar mass) if compared to our results at $z \sim 1.2$. The evolution in the smTFR computed using IMAGES dataset is very similar (within the errors) to the evolution we report at higher redshift (-0.36 ± 0.11 dex at $z \sim 1.2$). There are important issues to be taken into account when interpreting these values. The original evolution claimed by Flores et al. (2006) on the same data-set was consistent with no, or marginal evolution. Other authors, using traditional slit spectroscopy, reached the same qualitative conclusion of no/mild evolution up to redshift $z \simeq 1$ (e.g., Weiner et al. 2006; Conselice et al. 2005; Fernández Lorenzo et al. 2010). The IMAGES galaxies have large seeing and coarse spatial resolution due to the FLAMES instrument (Puech et al. 2010). Furthermore, the *lack* of evolution in the *baryonic* (star+gas) Tully-Fisher relation reported by Puech et al. (2010) using the same IMAGES sample and a gas fraction at $z \sim 0.6$ similar to the values of nearby galaxies, would imply a minimal, if not negligible evolution of the stellar-mass TFR (Dutton et al. 2011). All these points would therefore suggest an over-estimation of the evolution of the stellar Tully-Fisher relation by Puech et al. (2008) and an evolution of the smTF relation of IMAGES data of the order of -0.1 dex only, instead of the estimated -0.34 dex (Dutton et al. 2011).

If we compare our best fit with the Bell & de Jong (2001) calibration at $z \sim 1.2$ of the four SINS galaxies by Cresci et al. (2009) at similar redshifts, it is consistent with no evolution of the zero point. These four galaxies are very massive ($\sim 10^{11} \mathcal{M}_{\odot}$) with velocities around ~ 250 km s^{-1} where the two calibrations give similar estimates. At larger redshift, Cresci et al. (2009) found a shift in the stellar masses at fixed velocity of -0.41 ± 0.11 dex compared to the $z = 0$ Bell & de Jong (2001) calibration. Similar evolution is observed with the calibration by Pizagno et al. (2007), or -0.44 ± 0.11 dex (Cresci priv. comm.). The absence of discrepancy when taking two different calibrations is expected giving the properties of the analysed SINS galaxies. They are very massive and fast rotators and are located at the intersection between the two local relations in the stellar mass - velocity diagram. Gnerucci et al. (2011) using LSD/AMAZE galaxies show the possible build-up of the stellar mass TF relation at $z \sim 3$. Despite the large scatter of the correlation (~ 1.5 dex) they report a statistical shift of the zero point to their local relation of -1.29 dex (a very fast evolution, -0.88 dex, between $z \sim 2.2$ and 3 compared to more recent cosmic epochs).

Galaxies at high redshifts have a larger velocity dispersion and a higher fraction of turbulent motions (e.g., Genzel et al. 2008). To account for the large velocity dispersion that contributes to galactic kinematics at increasing redshift, we plot in the bottom panel of Fig. 4 the relation between the stellar mass and the S_{05} index. The S_{05} index is defined as follows: $S_{05} = \sqrt{(0.5 \times v_{rot}^2 + \sigma_0^2)}$, it accounts for the contribution of both ordered and turbulent motions (Kassin et al. 2007; Covington et al. 2010).

The cyan shaded area shows the 1σ error on the zero-point parameter, the cyan dotted and cyan dashed lines are the intrinsic and total scatters, respectively. Diagonal lines represent the best-fit relation by Kassin et al. (2007) at $z \sim 1$ (dot-dashed black line) and by Gnerucci et al. (2011) at $z \sim 3$ (dot-dashed ma-

genta line) calibrated using the slope by Kassin et al. (2007). We observe a tighter correlation with a reduced scatter than the classical smTF relation. Physically this smaller scatter of the distribution reinforces the recent results on the importance of chaotic motions to the galactic kinematics, and the larger contamination encountered in traditional long-slit spectroscopy.

Using the S_{05} index the rotators and non-rotators are located now in the same locus (bottom panel of Fig. 4). The $z \sim 1.2$ smTF$_{S05}$ is log(M$_\star$)= 4.46±0.07 + 2.92 × log(S$_{05}$) (with σ_{intr}=0.08 and σ_{tot}=0.45) when galaxies of both classes are included. If only rotating galaxies are considered (this is the correlation plotted in the figure), the relation can be written as log(M$_\star$)= 4.26±0.10 + 2.92 × log(S$_{05}$) (with σ_{intr}=0.13 and σ_{tot}=0.43). We therefore report a shift in stellar mass of −0.25 dex of the rotating MASSIV sample (or −0.45 dex including both dynamical classes) compared to Kassin et al. (2007) galaxies at $z \sim 1$ and of +0.35 dex (or +0.55 dex) to Gnerucci et al. (2011) galaxies at $z \sim 3$.

Figure 5 shows the relation between the baryonic mass and the velocities (top panel) and the ordered+chaotic motion components, quantified using the $S_{0.5}$ index (bottom panel). Based on our results we infer no evolution; that is to be compared with the conclusions reached by McGaugh (2005) in the local Universe implying a very marginal evolution of the content of the gaseous component with respect to nearby galaxies. Previous results on the baryonic TF relation using a data-set of integral field survey have been derived by Puech at al. (2010) who find no significant evolution compared to the local Universe. Based on this issue these authors claim for gas already in place at $z \sim 0.6$ with no need to advocate external gas accretion being the gas already bound to the gravity well of galaxies. Other interpretations are possible: if the growth with cosmic time of galactic velocities and masses happen along the scaling relation, as predicted by LCDM models, any apparent evolution can be observationally recognized.

6. Discussion and Conclusions

We have explored the relationships between galaxy size, mass, and internal velocity of the statistically representative MASSIV sample of 45 galaxies with near-infrared resolved kinematics at $1 < z < 1.6$., an unbiased sample of high-z star-forming galaxies (Contini et al. 2011).

Before the advent of the 3D integral field spectroscopy the possible sources of discordance in using these quantities include observational difficulties and selection effects (Portinari & Sommer-Larsen 2007). The higher fraction of morphological and kinematic disturbances in high-z galaxies compared to nearby objects may bias the real evolutionary effects. However, systematics and subtle selection effects also need to be taken into account when comparing with recent near-infrared resolved kinematics surveys. For example, the observations of the OSIRIS sample (Law et al. 2007, 2009; Wright et al. 2008) were assisted by adaptive optics to reach very high angular resolutions, but probing only the highest surface brightness emission. With this observing mode they sample smaller characteristic Hα radii (∼ 1.3 kpc) than those typically probed (∼ 3 kpc) in other similar surveys at comparable redshifts. The IMAGES survey (Hammer et al. 2007; Puech et al. 2008, 2010) samples both star-forming and more quiescent galaxies, but the coarse spatial resolution of FLAMES instrument requires meticulous correction methods to extract the maximum velocity. The SINS sample is the largest collection of galaxies at high-z, but extracted

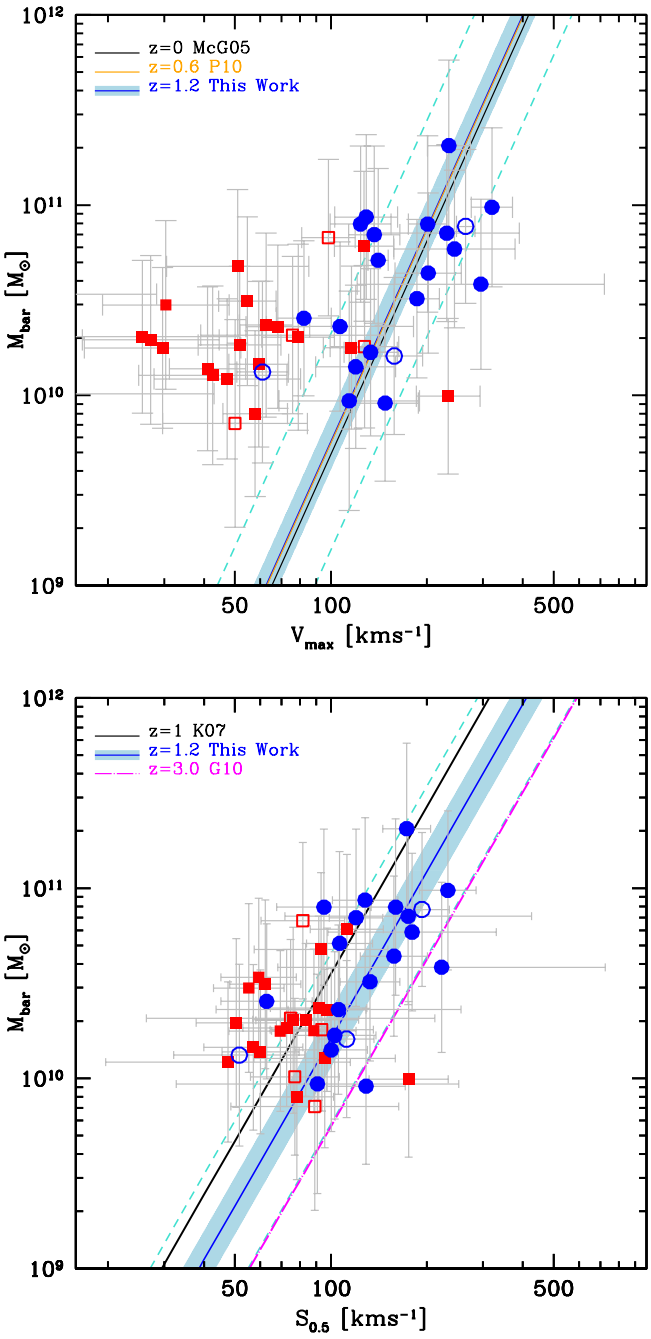

Fig. 5. The baryonic TF (bTF) relation versus the maximum velocity (top panel) and versus the $v + \sigma$ (or $S_{0.5}$) index (bottom panel). We overplot the best-fit relation of rotating galaxies (blue symbols) using the local slopes by McGaugh (2005) (plotted as solid black line in the top panel, McG05) and by Kassin et al. (2007) at $z \sim 1$ (plotted as solid black line in the bottom panel, K07). The other fit in the top panel is by Puech et al. (2010) (P10, $z \sim 0.6$, solid, orange line) and in the bottom panel by Gnerucci et al. (2011) ($z \sim 3$, long-dashed-dotted magenta line, G11). The cyan shaded area shows the 1σ error on the zero-point parameter (the intrinsic and total scatter is plotted as cyan dotted line and cyan dashed line, respectively). Symbols are as in Fig. 1.

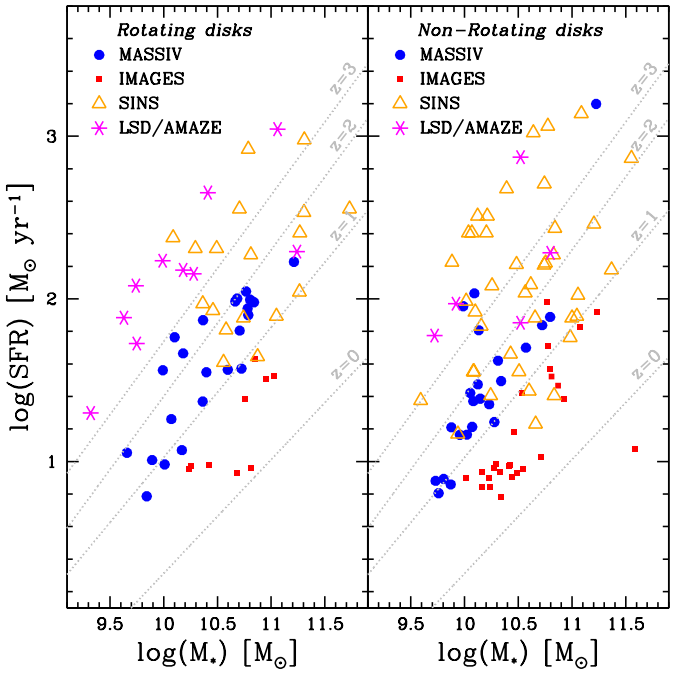

Fig. 6. Star Formation Rate versus stellar mass for rotators (left panel) and for non rotators (right panel) in the MASSIV ($1 < z < 1.6$, blue circle), IMAGES ($z \sim 0.6$, red square), SINS ($z \sim 2.2$, orange triangle) and LSD/AMAZE samples ($z \sim 3$, magenta asterisk). The grey dotted lines show the empirical main sequence of star-forming galaxies following Bouché et al. (2010) at different redshifts. All quantities have been opportunely rescaled to account for our Salpeter IMF.

from surveys with different selection criteria. The SINS sample used to analyse the relationship between stellar mass and velocity, represents galaxies detected with the highest signal-to-noise ratio: they are the most luminous/massive, fastest, and highly star-forming galaxies.

How some of these observational facts reflect on the physical interpretation is illustrated in the left panel of Fig. 6 where the star formation rate of rotating discs obtained by SED fitting in recent resolved kinematics surveys is plotted as a function of the stellar mass. The class of non-rotating/merging systems is shown in the right panel of the same figure. The main sequence of star-forming galaxies as defined by Bouché et al. (2010) is drawn at different redshifts. The IMAGES rotators lie below the sequence defined by the MASSIV rotators consistently rescaled in star formation rate and stellar mass given their later cosmic epoch (but covering a large interval of galactic properties), similarly high-z LSD/AMAZE rotating discs stay above the sequence. SINS rotators are highly star-forming objects and very massive, thus coincide with the massive, star-forming tail of the MASSIV galaxy distribution. The SINS properties can explain the mostly absent scatter in the Tully-Fisher relation by Cresci et al. (2009) compared to our scatter in the same relation (cf. our Fig. 4 with their Fig. 5). Contrary to what was expected, the difference in SFR between MASSIV and SINS galaxies cannot be attributed to the higher redshift and/or to the limits imposed on the minimum line flux to ensure detection (Contini et al. 2011). In this figure there is a larger dispersion of SINS rotators around the main sequence compared to other samples. This fact may be the consequence of at least two combined effects. The first one may be due to the heterogeneous SINS selection. The second effect may be physical, caused by an unexpected larger incidence of internal/external mechanisms (inflows/mergers, outflows/feedback) acting on both the spectrophotometric and dynamical properties of rotating discs. While we cannot discard the second hypothesis, it is unlikely that the same mechanisms acting on SINS galaxies at $z \sim 2$ are not at play a few Gyr later in MASSIV galaxies (assuming both samples are representative of the entire rotating disc population). Nevertheless, we can speculate that we witness the same phenomena acting with different efficiency on the various physical regimes (of galactic stellar mass, star-formation rate, etc.). Furthermore, comparing the SFR for rotators (left panel in Fig. 6) and non-rotators (right panel) for SINS and MASSIV surveys, it appears that non-rotating systems display similar ranges of SFR at $z \sim 1$ and $z \sim 2$, while it is not the case for rotating systems that exhibit higher SFR at $z \sim 2$ than at $z \sim 1$. Our results highlight the importance of the disc formation in the SFR mechanics between $z \sim 2$ and $z \sim 1$ (assuming these samples are representative of the entire rotating disc population). In summary, data-sets available so far (even those taking advantages from resolved spectroscopy), are spectroscopic surveys that pass through a natural pre-selection from one, or several photometric catalogues. As a consequence the comparison between samples remains difficult. At present, firm conclusions based on comparisons with other surveys, that are differently plagued by systematics in the galaxy properties determinations (e.g., different selection effects, quantities obtained at different wavelengths and with different assumptions), should be formulated with caution.

In this work we aim at exploring statistical issues. We analysed a large representative catalogue of galaxies with well-known selection functions, that is based on flux-limited multiple fields of a homogeneous redshift survey observed at higher spectral resolution, but with sufficient spatial resolution probing typical scales of ∼ 5 kpc. Our results are the following.

The MASSIV galaxies show a correlation between dynamical and stellar mass with an offset interpreted as a fraction of gas mass of the order of 20-25% of the stellar mass at $z \sim 1.2$. A similar amount of gas mass is obtained using the Kennicutt-Schmidt formulation. This fraction of gas mass evolves mildly for the last 8 Gyr. It is reinforced by the lack of a statistically significant evolution of our baryonic Tully-Fisher relation. Instead, the disagreement in the gas estimates using the two approaches for non-rotating galaxies, suggests different properties of dark matter halos in rotators and systems not supported by rotation at high-z, similarly to what is prescribed for nearby objects. The stellar mass in MASSIV galaxies is correlated with the incidence to be a rotator, or a non-rotator, with non-rotating galaxies presenting a lower content of stellar mass at fixed gas content and dynamical mass, but not at fixed star-formation rate. Furthermore, non-rotators are more compact in the extent of the stellar component than rotators, but not in the gas extent.

We obtained correlations between galaxy size, mass, and internal velocity, as observed in the local Universe and indicated by previous results, but the size - mass and size - velocity relations are weak at $1 < z < 1.6$. While individual galactic properties are in fact evolving with time as advocated by most recent results of large galaxy surveys, the marginal change observed in the relationships linking the three fundamental quantities analysed in this work – size, mass, and internal velocity – suggests an evolution along these relations. This picture agrees well with cosmological N-body/hydrodynamical simulations by e.g., Portinari & Sommer-Larsen (2007) and Firmani & Avila-Reese

(2009). We do not confirm the hypothesis of a strong, positive evolution in the size - stellar mass and size - velocity relations with discs being evenly smaller with look-back time at fixed stellar mass or velocity. Our results do not imply an abnormal evolution in the galactic spin as previously reported by Bouché et al. (2007). However, we discover a large spread in the distributions, the scatter is quite reduced for non-rotating galaxies when including the contribution of turbulent motions (with the S_{05} index) in the relations involving the velocities. It is in disagreement with the hypothesis that large scatters in the low-velocity regime are due to disturbed or compact objects, as suggested by Covington et al. (2010). In fact, restricting our analysis to regularly rotating discs that sample a large range of stellar masses and sizes, we report a persisting scatter. Its origin is likely intrinsic, and possibly caused by complex physical mechanism(s) at work in our stellar mass/luminosity regime and redshift range. At the present stage of the MASSIV survey and given the typical scale (~ 5 kpc) used to trace the resolved kinematics, we are not able to investigate further the mechanism(s) driving these galactic properties. It is still a matter of debate whether we trace more turbulent discs where star formation is the energetic driver (e.g., Lehnert et al. 2009; Green et al. 2010), or we are influenced by the infall of accreting matter, and/or large collisional clumps (e.g., Law et al. 2007, 2009; Genzel et al. 2011), and/or merger events (e.g., Hammer et al. 2011).

Further progress will be possible at the completion of our survey, doubling the statistics with galaxies in our highest ($z > 1.2$) redshift range. However, some issues will require larger-scale surveys of kinematically resolved galaxies. Future surveys should be able to assess firm conclusions about the cosmic evolution of the slope of the size/mass/velocity fundamental relations of discs at $z > 1$. There is also the impelling request to establish the imprint of the environmental effect at work, preferentially at certain stellar mass regimes. Of course, the stellar component and ionized gas content of galaxies offer a partial view of the galaxy formation and evolution, which must be supplemented with the properties of the cold/molecular phase of the interstellar component. We need to comprehend under which conditions, and how efficient, the gas is converted into stars through cosmic epochs. The relation between the galactic properties probed in our survey and the characteristics of the gas reservoir will offer a crucial step to link the data to models of galaxy formation.

7. Acknowledgments

DV acknowledges the support from the INAF contract PRIN-2008/1.06.11.02. This work has been partially supported by the CNRS-INSU and its Programme National Cosmologie-Galaxies (France) and the French ANR grant ANR-07-JCJC-0009.

References

Arnouts, S., Walcher, C. J., Le Fèvre, O., et al. 2007, A&A, 476, 137
Baker, A. J., Tacconi, L. J., Genzel, R., Lehnert, M. D., & Lutz, D. 2004, ApJ, 604, 125
Bamford, S. P., Milvang-Jensen, B., & Aragón-Salamanca, A. 2007, MNRAS, 378, L6
Bell, E. F. & de Jong, R. S. 2001, ApJ, 550, 212
Bell, E. F., McIntosh, D. H., Katz, N., & Weinberg, M. D. 2003, ApJS, 149, 289
Blumenthal, G. R., Faber, S. M., Primack, J. R., & Rees, M. J. 1984, Nature, 311, 517
Bonnet, H., Abuter, R., Baker, A., et al. 2004, The Messenger, 117, 17
Bouché, N., Cresci, G., Davies, R., et al. 2007, ApJ, 671, 303
Bouché, N., Dekel, A., Genzel, R., et al. 2010, ApJ, 718, 1001
Bruzual, G. & Charlot, S. 2003, MNRAS, 344, 1000
Bundy, K., Ellis, R. S., Conselice, C. J., et al. 2006, ApJ, 651, 120
Conselice, C. J., Bundy, K., Ellis, R. S., et al. 2005, ApJ, 628, 160
Contini, T., Garilli, B., Le Fevre, O., et al. 2011, ArXiv e-prints
Courteau, S. 1997, AJ, 114, 2402
Covington, M. D., Kassin, S. A., Dutton, A. A., et al. 2010, ApJ, 710, 279
Cowie, L. L., Songaila, A., Hu, E. M., & Cohen, J. G. 1996, AJ, 112, 839
Cresci, G., Hicks, E. K. S., Genzel, R., et al. 2009, ApJ, 697, 115
Cucciati, O., Tresse, L., Ilbert, O., et al. 2011, ArXiv e-prints
Daddi, E., Bournaud, F., Walter, F., et al. 2010, ApJ, 713, 686
Dalcanton, J. J., Spergel, D. N., & Summers, F. J. 1997, ApJ, 482, 659
de Jong, R. S. & Lacey, C. 2000, ApJ, 545, 781
Dekel, A., Birnboim, Y., Engel, G., et al. 2009, Nature, 457, 451
Dutton, A. A., van den Bosch, F. C., Dekel, A., & Courteau, S. 2007, ApJ, 654, 27
Dutton, A. A., van den Bosch, F. C., Faber, S. M., et al. 2011, MNRAS, 410, 1660
Eisenhauer, F., Abuter, R., Bickert, K., et al. 2003, in Society of Photo-Optical Instrumentation Engineers (SPIE) Conference Series, Vol. 4841, Society of Photo-Optical Instrumentation Engineers (SPIE) Conference Series, ed. M. Iye & A. F. M. Moorwood, 1548–1561
Epinat, B., Amram, P., & Marcelin, M. 2008, MNRAS, 390, 466
Epinat, B., Contini, T., Le Fèvre, O., et al. 2009, A&A, 504, 789
Epinat, B., Tasca, L., Amram, P., et al. 2012, ArXiv e-prints
Erb, D. K., Steidel, C. C., Shapley, A. E., et al. 2006, ApJ, 646, 107
Fernández Lorenzo, M., Cepa, J., Bongiovanni, A., et al. 2010, A&A, 521, A27+
Firmani, C. & Avila-Reese, V. 2000, MNRAS, 315, 457
Firmani, C. & Avila-Reese, V. 2009, MNRAS, 396, 1675
Flores, H., Hammer, F., Puech, M., Amram, P., & Balkowski, C. 2006, A&A, 455, 107
Fontana, A., Pozzetti, L., Donnarumma, I., et al. 2004, A&A, 424, 23
Fontana, A., Salimbeni, S., Grazian, A., et al. 2006, A&A, 459, 745
Förster Schreiber, N. M., Genzel, R., Bouche, N., et al. 2009, ArXiv e-prints
Förster Schreiber, N. M., Genzel, R., Lehnert, M. D., et al. 2006, ApJ, 645, 1062
Franzetti, P., Scodeggio, M., Garilli, B., Fumana, M., & Paioro, L. 2008, in Astronomical Society of the Pacific Conference Series, Vol. 394, Astronomical Data Analysis Software and Systems XVII, ed. R. W. Argyle, P. S. Bunclark, & J. R. Lewis, 642–+
Garilli, B., Le Fèvre, O., Guzzo, L., et al. 2008, A&A, 486, 683
Garrido, O., Marcelin, M., Amram, P., et al. 2005, MNRAS, 362, 127
Genel, S., Genzel, R., Bouché, N., et al. 2008, ApJ, 688, 789
Genzel, R., Burkert, A., Bouché, N., et al. 2008, ApJ, 687, 59
Genzel, R., Newman, S., Jones, T., et al. 2011, ApJ, 733, 101
Genzel, R., Tacconi, L. J., Eisenhauer, F., et al. 2006, Nature, 442, 786
Gnerucci, A., Marconi, A., Cresci, G., et al. 2011, A&A, 528, A88+
Green, A. W., Glazebrook, K., McGregor, P. J., et al. 2010, Nature, 467, 684
Hammer, F., Puech, M., Chemin, L., Flores, H., & Lehnert, M. D. 2007, ApJ, 662, 322
Hammer, F., Puech, M., Flores, H., et al. 2011, ArXiv e-prints
Kassin, S. A., Weiner, B. J., Faber, S. M., et al. 2007, ApJ, 660, L35
Kennicutt, R. C. 1998a, ARA&A, 36, 189
Kennicutt, Jr., R. C. 1998b, ApJ, 498, 541
Larkin, J., Barczys, M., Krabbe, A., et al. 2006, New Astronomy Review, 50, 362
Law, D. R., Steidel, C. C., Erb, D. K., et al. 2007, ApJ, 669, 929
Law, D. R., Steidel, C. C., Erb, D. K., et al. 2009, ApJ, 697, 2057
Le Fèvre, O., Vettolani, G., Garilli, B., et al. 2005, A&A, 439, 845
Lehnert, M. D., Nesvadba, N. P. H., Tiran, L. L., et al. 2009, ApJ, 699, 1660
Markwardt, C. B. 2009, in Astronomical Society of the Pacific Conference Series, Vol. 411, Astronomical Data Analysis Software and Systems XVIII, ed. D. A. Bohlender, D. Durand, & P. Dowler, 251
Mathewson, D. S., Ford, V. L., & Buchhorn, M. 1992, ApJS, 81, 413
McCracken, H. J., Radovich, M., Bertin, E., et al. 2003, A&A, 410, 17
McGaugh, S. S. 2005, ApJ, 632, 859
Meurer, G. R., Carignan, C., Beaulieu, S. F., & Freeman, K. C. 1996, AJ, 111, 1551
Mo, H. J., Mao, S., & White, S. D. M. 1998, MNRAS, 295, 319
Modigliani, A., Hummel, W., Abuter, R., & et al. 2007, ArXiv e-prints
Noordermeer, E. & Verheijen, M. A. W. 2007, MNRAS, 381, 1463
Peng, C. Y., Ho, L. C., Impey, C. D., & Rix, H.-W. 2002, AJ, 124, 266
Persic, M. & Salucci, P. 1991, ApJ, 368, 60
Persic, M., Salucci, P., & Stel, F. 1996, MNRAS, 281, 27
Pizagno, J., Prada, F., Weinberg, D. H., et al. 2005, ApJ, 633, 844
Pizagno, J., Prada, F., Weinberg, D. H., et al. 2007, AJ, 134, 945
Portinari, L. & Sommer-Larsen, J. 2007, MNRAS, 375, 913
Pozzetti, L., Bolzonella, M., Lamareille, F., et al. 2007, A&A, 474, 443
Puech, M., Flores, H., Hammer, F., et al. 2008, A&A, 484, 173
Puech, M., Hammer, F., Flores, H., et al. 2010, A&A, 510, A68+
Puech, M., Hammer, F., Lehnert, M. D., & Flores, H. 2007, A&A, 466, 83
Queyrel, J., Contini, T., Kissler-Patig, M., et al. 2011, ArXiv e-prints

Robertson, B. E. & Bullock, J. S. 2008, ApJ, 685, L27
Rodrigues, M., Hammer, F., Flores, H., et al. 2008, A&A, 492, 371
Salpeter, E. E. 1955, ApJ, 121, 161
Schiminovich, D. 2008, in American Institute of Physics Conference Series, Vol. 1035, The Evolution of Galaxies Through the Neutral Hydrogen Window, ed. R. Minchin & E. Momjian, 180–185
Schmidt, M. 1959, ApJ, 129, 243
Stark, D. P., Swinbank, A. M., Ellis, R. S., et al. 2008, Nature, 455, 775
Tacconi, L. J., Genzel, R., Neri, R., et al. 2010, Nature, 463, 781
Tresse, L., Ilbert, O., Zucca, E., et al. 2007, A&A, 472, 403
Trujillo, I., Förster Schreiber, N. M., Rudnick, G., et al. 2006, ApJ, 650, 18
Tully, R. B. & Fisher, J. R. 1977, A&A, 54, 661
Vergani, D., Scodeggio, M., Pozzetti, L., et al. 2008, A&A, 487, 89
Verheijen, M. A. W. 2001, ApJ, 563, 694
Walcher, C. J., Lamareille, F., Vergani, D., et al. 2008, A&A, 491, 713
Weiner, B. J., Willmer, C. N. A., Faber, S. M., et al. 2006, ApJ, 653, 1049
Williams, R. J., Quadri, R. F., Franx, M., et al. 2010, ApJ, 713, 738
Wright, S. A., Larkin, J. E., Law, D. R., et al. 2008, ArXiv e-prints
Zucca, E., Ilbert, O., Bardelli, S., et al. 2006, A&A, 455, 879